

SPUTTERED UHF ZINC OXIDE TRANSDUCERS

BY

John T. Liebmann, B.Eng.

SPUTTERED UHF ZINC OXIDE TRANSDUCERS

by

John T. Liebmann, B.Eng.

**A thesis submitted to the Faculty of Graduate Studies and Research
in partial fulfillment of the requirements for the degree of
Master of Engineering.**

**Department of Electrical Engineering,
McGill University,
Montreal, Quebec,**

June, 1968

ABSTRACT

This work describes the preparation of zinc oxide thin films for use as ultrasonic transducers. The properties of zinc oxide are summarized and the theory and methods of thin film deposition are discussed. The design of a reactive sputtering system is described and the films produced with this system are evaluated with respect to their mechanical, electrical and piezoelectric properties. A circuit model for the general case of a transducer of finite conductivity is derived and the results of calculations of electromechanical conversion efficiency and insertion loss, using this model, are presented for various electrical terminations.

ACKNOWLEDGEMENTS

The author wishes to express his appreciation to the Northern Electric Company Limited for their financial support and to the Applied Chemistry Division of the National Research Council for their help in crystal structure evaluation.

Many thanks are due to Dr. E.L. Adler for his generous help and guidance, to Mr. J. Foldvari for constructing the sputtering apparatus and Mr. S. Sizgoric for his many suggestions.

TABLE OF CONTENTS

	<u>Page</u>
ABSTRACT	i
ACKNOWLEDGEMENTS	ii
TABLE OF CONTENTS	iii
TABLE OF ILLUSTRATIONS	v
CHAPTER I INTRODUCTION	1
CHAPTER II PIEZOELECTRIC MATERIALS	3
2.1 The Piezoelectric Constant	3
2.2 Electromechanical Coupling Constant	6
2.3 Properties of ZnO	8
2.3.1 Crystal Structure	8
2.3.2 Electrical and Mechanical Properties	14
CHAPTER III ANALYSIS OF TRANSDUCER PERFORMANCE	17
3.1 Introduction	17
3.2 The Perfect Dielectric Transducer	18
3.3 Extrinsic Semiconductor Transducer	23
3.4 Insertion Loss Calculations	30
3.5 Results of Computations	32
CHAPTER IV METHODS OF DEPOSITION	36
4.1 Introduction	36
4.2 The Glow Discharge	37
4.3 Sputtering Mechanisms	40
4.4 Methods of Sputtering	44
CHAPTER V EXPERIMENTAL APPARATUS AND PROCEDURES	49
5.1 Sputtering Unit	49
5.2 Electrical Connections	49
5.3 Operating Procedures	51
5.4 Sputtering Difficulties	53
5.5 Adhesion of Gold to Substrate	54
5.6 Substrate Cleaning	54
5.7 Thickness Measurements	55
5.8 Determination of Insertion Loss	57
CHAPTER VI EXPERIMENTAL RESULTS	59
6.1 The Effect of Sputtering on Different Cathodes	59
6.2 Establishment of the System Constant	60
6.3 Effect of Temperature on the System Constant	63
6.4 Effect of Oxygen on System Constant	65

6.5	Angle of Ion Incidence	66
6.6	Resistivity of the Deposited Films	66
6.7	Crystal Structure of the Deposits	68
6.8	Contaminants	72
6.9	Discussion	73
CHAPTER VII	CONCLUSIONS	74
REFERENCES		76

TABLE OF ILLUSTRATIONS

Figure 1	Crystal Structure of ZnS and Related Compounds	Page 1
Figure 2	ZnO Crystal Cut Along the (1210) Plane	Page 13
Figure 3	Electromechanical Model of Dielectric Piezoelectric Transducer	Page 22
Figure 4	Electrical Equivalent Circuit of Semiconducting Transducer	Page 31
Figure 5	Conversion Loss of Continuously Tuned Transducer	Page 34
Figure 6	Insertion Loss of Untuned and of Inductively Tuned Transducer	Page 35
Figure 7	V - I Characteristic of Glow Discharge	Page 39
Figure 8	Mean Free Path in Argon	Page 39
Figure 9	Yield as a Function of Atomic Number in Argon	Page 39
Figure 10	Basic Sputtering Configurations	Page 43
Figure 11	The Sputtering Unit	Page 52
Figure 12	Block Diagram of PEM Setup	Page 58
Figure 13	Rate of Deposition vs. Cathode Voltage	Page 61
Figure 14	Rate of Deposition as a Function of Cathode to Substrate Distance and Pressure	Page 62
Figure 15	Variation of System Constant with Substrate Temperature	Page 62
Figure 16	Variation of System Constant with Oxygen Content of Sputtering Gas	Page 64
Figure 17	Effect of the Angle of Bombardment	Page 64
Figure 18	Relationship between the Resistivity of ZnO Films and Growth Rate	Page 67
Figure 19	RED Picture of ZnO Film Deposited from Small Area Cathode	Page 70

Figure 20	RED Picture of ZnO Film Deposited from Large Area Cathode	Page 70
Figure 21	RED Pattern of Sputtered Gold Deposit	Page 70
Figure 22	Crystal Orientation of ZnO Films	Page 72

CHAPTER I

INTRODUCTION

Due to the ever widening use of ultrasound for industrial and research purposes, there is a strong interest in the development of more efficient transducers. Ultrasonic cleaning, underwater sonar, ultrasound for fault finding in metals, etc. have been used for some time, but these applications can tolerate relatively large power losses in conversion from electrical to sound energy and use ultrasound mainly in the lower frequency range, below a few megacycles. Since the discovery of ultrasonic amplifiers in the early 1960's⁷ and also due to the need for miniaturized delay lines with long delay times for electronic applications, it became necessary to fabricate transducers usable up to several gigahertz in frequency with a low conversion loss. Transducers made of piezoelectric materials provide for conversion in either direction with equal efficiency. Their small size and lack of moving parts permit easy handling and with the use of thin film technology their manufacture is becoming economically feasible.

The theory of piezoelectric transducers was very comprehensively presented by Berlincourt and Jaffe³ for dielectric materials, and the propagation of waves in piezoelectric semiconductors was worked out by Hutson and White³⁰. As is generally the case, theory is far ahead of technology in the field of high frequency transducers. It was shown by May³⁸, that zinc oxide and cadmium sulphide are two of the most suitable materials for the construction of these devices, with the former preferable in the frequency range above several hundred megahertz, but fabrication techniques have not yet

caught up with the demand.

For most efficient operation these transducers must be made very thin, few microns in thickness, and especially for zinc oxide the methods of thin film deposition are not yet reliable. The structural properties of vacuum deposited CdS films were under examination for more than ten years and Foster³⁹ and de Klerk⁴⁰ have successfully produced high efficiency transducers of vapour deposited CdS. Rozgonyi and Foster³⁶ have made working ZnO transducers by sputtering the compound, and Wanuga⁴¹ experimented with reactive sputtering of zinc in a mixture of argon and oxygen, but the structure of the films was extremely sensitive to deposition parameters and reproducibility left much to be desired.

This thesis develops an electrical circuit model for the general case of the piezoelectric transducer of finite conductivity, which permits the quick determination of conversion efficiency and insertion loss under any loading conditions. The experimental portion of the thesis describes the design details of a sputtering apparatus, created specifically for the reactive sputtering of ZnO thin films, and the effect of the various deposition parameters on the electrical, mechanical and crystallographic properties of these films from the point of view of their usefulness as transducers.

CHAPTER II

PIEZOELECTRIC MATERIALS

2.1 The Piezoelectric Constant

In order to gain insight into the process of selecting materials for transducers, it is necessary to understand the causes of piezoelectricity.

The polarization of a material in an external electric field can result in either the rearrangement of individual nuclei and their electrons to form dipoles, or in the realignment of already existing dipoles. In either case the dimensions of the material change. The application of a mechanical stress however merely effects the position of mass points without creating new dipoles, hence there will be no potential difference caused by it between two points on the crystal if there were no permanent dipoles to begin with.

All dielectrics are polarizable in an electric field and will show the one way effect of dimensional change (electrostriction), but only crystals with at least partial ionic bonding will show piezoelectric properties, ie. an equal but opposite response to electrical and mechanical excitations. In order for this to happen the dipoles must not be randomly oriented, or in the case of a single crystal there must not exist a center of symmetry, otherwise the individual charges will cancel out. Thus, by excluding crystals with a center of symmetry there remain 20 crystal classes in which piezoelectricity may occur. For a polar axis to exist, the individual dipole moment vectors in the unit cell must add up to a permanent moment. This moment is dependent in magnitude on the lattice dimensions and thus piezoelectric crystals, possessing neither a reflection plane, nor a two fold axis perpendicular to the direction in question are also pyroelectric. Ten of the 20 piezoelectric

classes are pyroelectric.

Dipole moments parallel to an axis of symmetry will not produce piezoelectric effects when excited perpendicular to this axis but will react to excitation along the axis. In the case of a triad axis even normal fields will produce a reaction, since pressure in this direction will spread the angle between one pair of dipoles, but decrease it between the other two. If the electric polarization P is given in a 3 dimensional orthogonal coordinate system by

$$P_i = \sum_j d_{ij} T_j, \quad i = 1, \dots, 3 \quad j = 1, \dots, 6$$

where T_j is the applied mechanical stress, then the piezoelectric properties of the crystal are described by the matrix :

$$d = \begin{pmatrix} d_{11} & \dots & \dots & \dots & \dots & d_{16} \\ \cdot & & & & & \cdot \\ d_{31} & \dots & \dots & \dots & \dots & d_{36} \end{pmatrix}.$$

The elements of this matrix can be derived by inspection of the dipole representation of crystals.

Consider, for example, zinc sulphide, which exists either as a cubic zinc blend, (sphalerite), or as hexagonal wurtzite. The similarity between the two structures becomes apparent if one orients the space diagonal of the former parallel to the c -axis of the latter, (Figure 1.). Both of these structures can be built up from double-tetrahedral building blocks, (Figure 1d.). It is evident that, from the point of view of crystal symmetry, either form can be piezoelectric. Pressure along the c -axis will compress the central pair and at the same time increase the angle the other dipoles make with the c -axis. This change increases

the moment of the central pair while the c-axial components of the balancing moments decrease, as a result of this $d_{33} \neq 0$ but $d_{31} = d_{32} = 0$. Pressure along, say, the a-axis will decrease the angle the side pairs make with the c-axis but will not change the compensating moment of the central pair, making $d_{23} = d_{13} \neq 0$. Also while pressure along the a- or b-axis would produce a net moment change from either bottom or top tetrahedra alone, these effects from the two together form an antiparallel pair and therefore $d_{11} = d_{12} = d_{21} = d_{22} = 0$.

Using these simple symmetry considerations one can quickly find, that the only nonzero piezoelectric coefficients for these two crystal classes are : d_{33} ; $d_{31} = d_{32}$ and $d_{15} = d_{24}$ ¹. At the same time it also becomes apparent that of these two structures only the wurtzite is pyroelectric, since here the Zn and S ions are always above each other in the c-direction, (the building block in Figure 1 depicts the sphalerite case). This results in the formation of additional vertical dipole pairs, causing a permanent electrostatic compression of the crystal, creating a polar axis. Other zinc compounds, ZnO, ZnSe, ZnTe behave similarly, but ZnO is found in the wurtzite configuration only. This is mainly due to the fact that of these four ZnO possess the strongest ionic attraction and therefore assumes the closest packed structure. The interatomic distance along the c-axis is about 5% shorter in ZnO than in the others². Viewing the structures one can also deduce that the temperature dependence of the piezoelectric coefficients must be small (inspite of pyroelectric polarization), since random motion of the ions and slight changes in lattice dimensions will not appreciably influence the way in which the dipole moments balance out. ✕

2.2 Electromechanical Coupling Constant

The magnitude of the piezoelectric constant alone does not determine the usefulness of a material for transducer fabrication. In building such a device one is mainly concerned with the conversion of energy from one form into another and a figure of merit assigned to these substances should depend on the portion of electrical energy that is extractable from them as mechanical energy, and vice-versa. The factor describing this relationship is the electro-mechanical coupling constant "K".

If one neglects thermal and magnetic effects, then the internal energy of a system is given by

$$U = (1/2) S_i T_i + (1/2) D_m E_m ; \quad \begin{matrix} i = 1, \dots, 6 \\ m = 1, \dots, 3 \end{matrix}$$

where S = strain; T = stress; D = electric displacement and E = electric field. The thermodynamic equations of state are :

$$T = c^D S - h D,$$

$$E = - h S + \beta D.$$

These are tensor equations and therefore in the usual summation convention

$$U = (1/2) S_i c_{ij}^D S_j + [(1/2) S_i \cdot (-h_{ij})] \cdot D_j + (1/2) S_i \cdot (-h_{ij}) \cdot D_j] \\ + (1/2) D_i \beta_{ij} D_j$$

$$U = U_{\text{elastic}} + 2 U_{\text{coupled}} + U_{\text{dielectric}} , \quad K = U_c / U_e U_d .$$

For the case of one dimensional strain parallel to the c-axis

$$K_{33} = h_{33} / c_{33}^D \beta_{33} = h_{33} e_{33}^S / c_{33}^D .$$

The coupling constant, in general, depends on the mode of operation, but under identical forms of excitation it is the figure of merit best suited for the comparison of different materials³. The choice is further influenced by several other factors as well, such as mechanical strength, power-handling capacity, dependence of properties on ambient conditions (like the coefficient of thermal expansion) and, of course, availability and economic considerations.

In low-frequency, high-power applications piezoelectric ceramics are widely used, for high-frequency and low-loss situations, however, they are not well suited. By deriving an electromechanical model of the loaded transducer one can express the relation between applied electric field and the delivered stress. Maximizing this relationship with respect to device dimensions it is found that the highest transduction efficiency is achieved when the length of the transducer is equivalent to a half wavelength of the generated ultrasound, if excitation is parallel to wave propagation. For the gigacycle range of frequencies this means that the device will be only a few microns thick. It is not only difficult to prepare such a device, but the material has to have good enough mechanical properties to withstand whatever subsequent handling is needed.

Since the idea of depletion layer transducers emerged, and since acoustic amplifiers were discovered, most of the attention became centered on the relatively good piezoelectric semiconducting compounds of cadmium and zinc.

2.3 The Properties of ZnO

2.3.1 Crystal Structure

Of the above mentioned compounds zinc oxide has the highest electroelastic coupling coefficient, is hard and strong enough to be useful in thin plate or film form, and its thermal properties (high melting point, expansion coefficient reasonably close to those of the most often used delay media), and sufficient chemical stability make it the best present day choice for hypersonic transducers.

Up to the time of it being considered for its piezoelectric properties, ZnO had relatively few uses. Some detailed investigations of its characteristics were carried out in the late 1940's, mainly because of interest in its photoconductivity³¹. At this time, however, the material was not available in large crystals, only in the form of compressed powder. For crystallographic studies it is advantageous to use large single crystals and most known methods produce needle - like crystals of rather small size, with the longest dimension along the c-axis. Growth in the "a" and "b" directions is very slow and rarely exceeds 1-mm, but plate-like crystals up to 1-cm long in the a-direction were successfully grown from a solution of ZnO in molten lead fluoride⁴. The more usual ways of producing it are by thermal oxidation of Zn films, by reactive evaporation, by reactive sputtering and by resputtering of compressed ZnO powder. Epitaxial growth from a direct evaporation of ZnO powder is difficult because of the high melting point (1800°C) and instability of the powder at high temperatures, resulting in considerable excess Zn in the deposit. Pure ZnO is white in the powder form, while larger pure crystals (with not more than 1% excess Zn) are colourless.

The crystal structure is hexagonal with a polar c-axis. Thus there is a difference between the (001) and (00 $\bar{1}$) directions and the opposite faces show different characteristics. The face with zinc as the surface layer shows negative charge under compression. In acids the oxygen surface etches much faster than the other and the high reaction rate usually masks etchpits. On the zinc surface hexagonal etchpits form readily with the apex below the surface and sides inclined at 45° - 50° to the c-axis, in strongly diluted acids the oxygen surface will show similar marks, but with the apex above the plane of the crystal. When grown from liquid solution or from the vapour phase the direction of growth is toward the oxygen surface.

It is interesting to develop a little further the simple piezoelectric considerations we have discussed earlier on the basis of the dipole mode of crystal representation. Consider once again the wurtzite structure but this time along a cut as shown in Figure 2.⁵ Suppose, that the crystal is under compression along the c-axis. Then the only major dimensional changes are in the quantities "u" and "r" while changes in the surface charge density Q are negligible. The sign of the piezoelectric effect is connected with the expression du/dr. In order to determine this ratio we will make use of the following constants :

$$\text{compliance} \quad S_{33} = 8.3 \times 10^{-12} \text{ m}^2/\text{N} \quad ; \quad S_{13} = -\mu \cdot S_{33}$$

$$\mu = 0.31 \quad ; \quad r = 1.96 \text{ \AA}$$

$$w = 1.98 \text{ \AA} \quad ; \quad u = 0.64 \text{ \AA} \quad ; \quad \alpha = 71.16^\circ$$

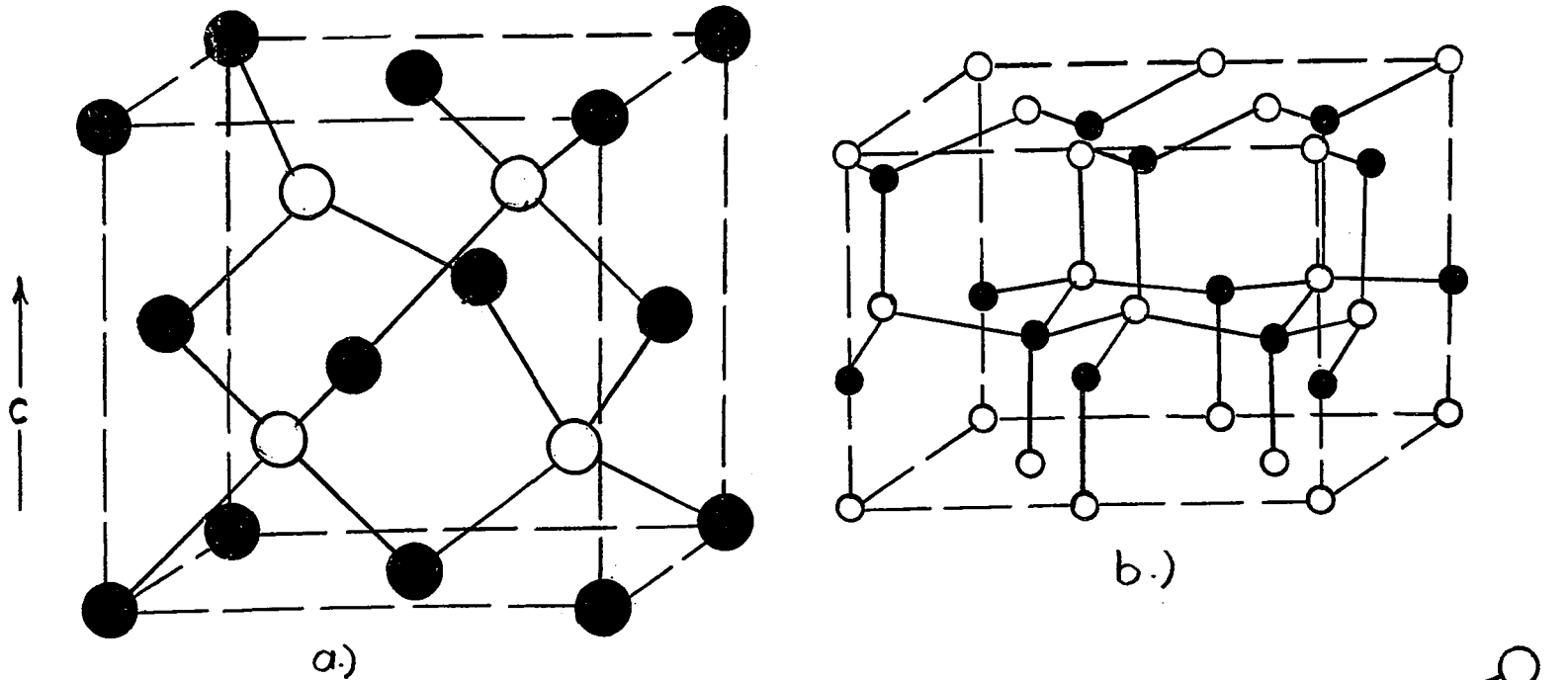
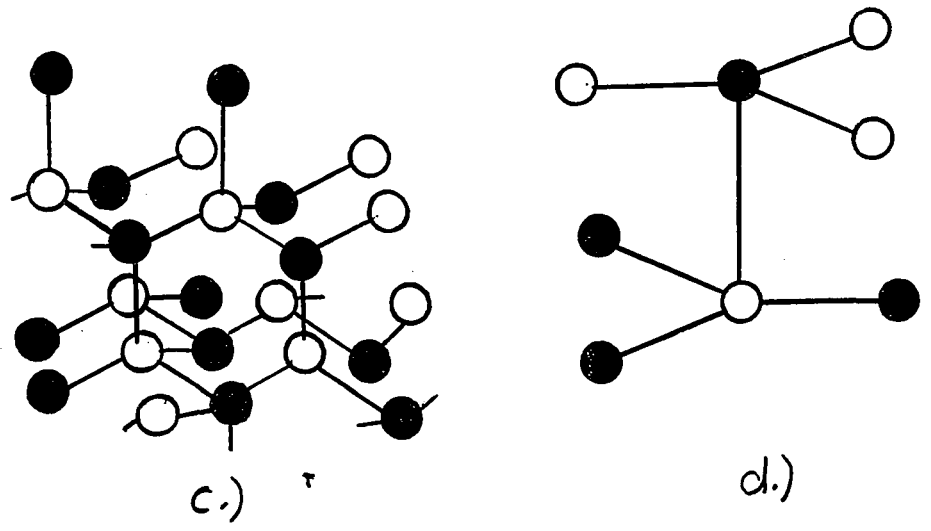


Fig. 1. Crystal structure of ZnS and related compounds. a) Sphalerite. b) Wurtzite. c) Sphalerite with [111] direction vertical. d.) Building block used in derivation of piezoelectric matrix.

● Zn ○ S



If the superscript ^(') denotes the change in the respective quantities after the application of unit pressure, then :

$$(r+u)' = (r+u) \cdot S_{33}$$

$$t' = t \cdot S_{13}$$

$$u = w \cos \alpha \quad \text{and} \quad t = w \sin \alpha$$

for small changes

$$\begin{aligned} \frac{du}{dr} = \frac{u'}{r'} &= \frac{S_{33} \mu w \sin^2 \alpha + w'}{(r+u) S_{33} \cos \alpha - S_{33} \mu w \sin^2 \alpha - w'} \\ &= \frac{(4.56 \times 10^{-22} \text{ m}^3/\text{N}) + w'}{(2.41 \times 10^{-22} \text{ m}^3/\text{N}) - w'} \end{aligned}$$

For the determination of the sign of the ionic charge, it is sufficient to give a lower limit for w' , let us say $w' = 0$; then :

$$\frac{du}{u} \bigg/ \frac{dr}{r} = \frac{u'}{u} \bigg/ \frac{r'}{r} > 6$$

Thus the piezoelectric effect is dominated by the change in "u" and, since the zinc surface is negatively charged in compression, the sign of the ionic charge of zinc must be positive. The size of this charge can be calculated from neutrality considerations. If the charge per unit area carried by the zinc surface is "Q" under no pressure conditions and the oxygen surface charge is " \overline{Q} ", then for neutrality one must have the interatomic electric fields :

$$E_u = (Q - \overline{Q}) / \epsilon \epsilon_0 \quad \text{and} \quad E_r = -Q / \epsilon \epsilon_0$$

For the potentials to be equal on the opposite faces of an n - double - layer lattice :

$$\frac{n(Q - \bar{Q})u}{\epsilon \epsilon_0} = (n-1) \frac{\bar{Q} \cdot r}{\epsilon \epsilon_0}$$

$$\text{and for } n = 1 \quad \bar{Q} = Q \cdot \frac{u}{u+r}$$

Let us now replace Q with the effective ionic charge q_e

$$\bar{Q} = \frac{2q_e}{a^2 \sqrt{3}} \cdot \frac{u}{u+r} ; \quad a = \text{lattice constant} \\ = 3.25 \text{ \AA}$$

On the application of pressure p_{33} the change in the compensating charge \bar{Q} is the measured piezoelectric constant d_{33}

$$d_{33} = \bar{Q}' = d\bar{Q}/dp_{33}$$

We made the assumption that compression effects on Q are very small, and therefore :

$$d_{33} = \frac{\partial \bar{Q}}{\partial u} u' + \frac{\partial \bar{Q}}{\partial r} r' \\ = \frac{2q_e}{a^2 \sqrt{3}} \cdot \frac{u \cdot r}{(u+r)^2} \left(\frac{u'}{u} - \frac{r'}{r} \right)$$

where $d_{33} = 1.2 \times 10^{-11}$ c/N. It was already shown that (r'/r) is negligible with respect to (u'/u) , and thus using the above given values for the different constants, one arrives at the minimum effective value of the ionic charge of $q_{e \text{ min}} = 1.1 e$. The upper limit is $q_{e \text{ max}} = 2.0 e$. If one defines the ionic portion of the bond as being zero for Z^{--} and 100% for Z^{++} , then the ZnO crystal can be looked upon as having a 77% ionic bond.

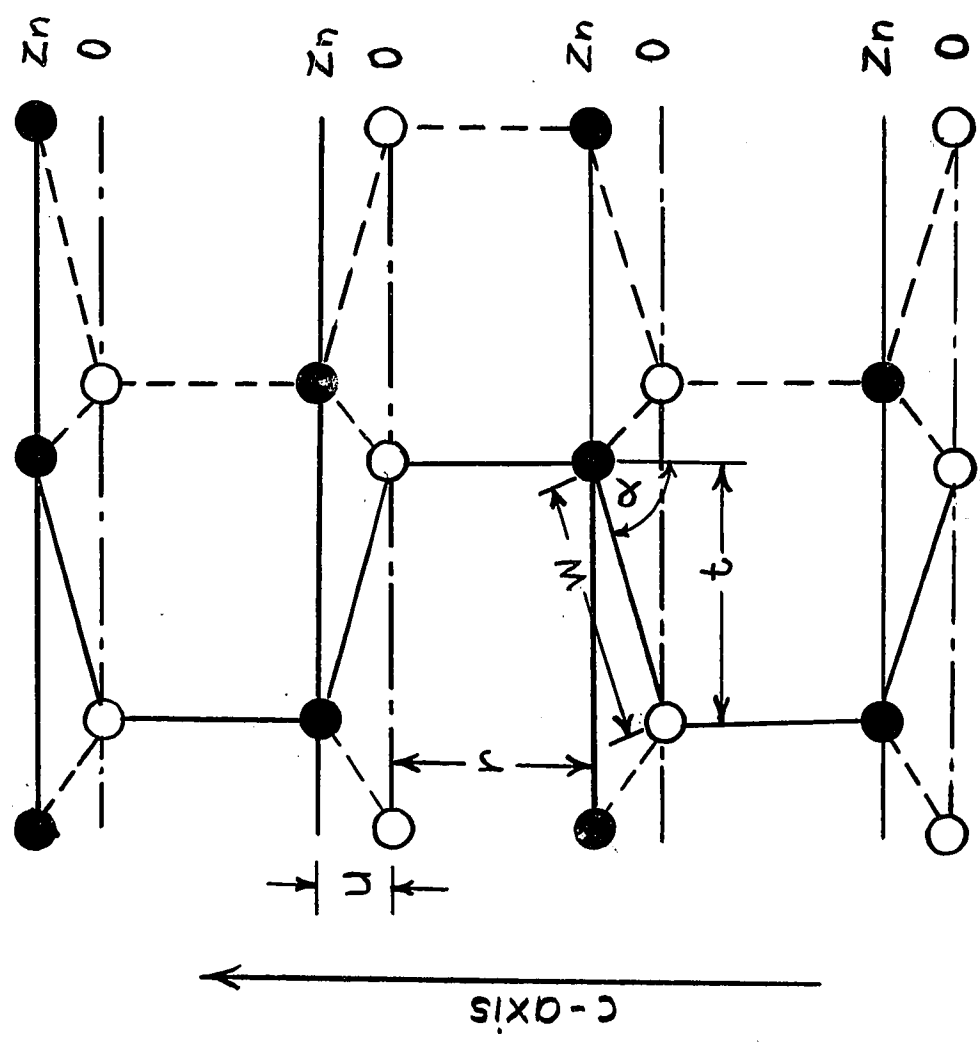


Fig. 2. ZnO crystal cut along the $[1\bar{2}10]$ plane.

2.3.2 Electrical and Mechanical Properties

High resistivity ZnO films, prepared by reactive sputtering⁶ show an exponential dependence of conductivity on temperature

$$\sigma = \text{const} \cdot e^{-E/kT}$$

with a value of E between 2 and 4 eV for different samples, up to about 450° C. Beyond this temperature the conductivity drops to very low values again if the heating takes place in air, but keeps on rising when heated in vacuum. These changes are not reversible during the first heating but are reversible after any subsequent tempering. This behaviour is explainable on the basis of the fact that in the lattice every Zn ion sits in the middle of an oxygen tetrahedra and vice versa, but when the building blocks are connected into a crystal, every second tetrahedra is unoccupied in the center. Thus the structure has large interstitial places and is prone to the absorbing of foreign atoms. From the conditions of growth of ZnO crystals it follows, that the probability of these interstitial sites being occupied by Zn or O, or both, is large. In fact it is seldom possible to grow crystals without some excess zinc. The conductivity is small initially inspite of this, because of the simultaneous presence of absorbed oxygen atoms which act as electron traps. During heating the oxygen diffuses to the surface and leaves the crystal, while thermal excitation increases the number of carriers. Beyond about 450° C there is the natural phenomena of resistivity increase due to lattice vibrations which becomes appreciable and parallel with it the excess zinc tends to become oxidized, thus reducing the number of carriers. (Note : the diffusion constant of O in the lattice is higher than that of Zn). Since most carriers come from the excess zinc, it is understandable that crystals, grown by whatever method, are usually n-type. To achieve very high resistivities, one usually dopes the crystal with lithium, which has a high diffusion constant in

this structure.

Optical absorption measurements, carried out by Mollwo⁴ at different temperatures show a linear dependence of the absorption edge up to about 700°K on temperature, and by extrapolating his results to 0°K a band gap of 3.35 eV was obtained. Watanabe⁴ observed that the colourless single crystals show a gradual orange colouration when heated, due to a shift of the fundamental absorption edge from the U.V. into the visible part of the spectrum. At wavelengths beyond one micron the absorption coefficient varies with the square of the wavelength, indicating an intraband free carrier absorption permitting the calculation of the effective mass giving $m^* \doteq 0.14m$. Other researchers¹², using different methods (phonon drag data) arrived at values of $m^* \doteq 0.10m - 0.40m$. Photoelectric emission experiments indicate an electron affinity for pure ZnO of 1.2 eV - 1.5 eV.

Measurements of mechanical properties are usually carried out with the help of ultrasonic techniques. Bateman⁸ used crystals grown by reactive evaporation and employed a high frequency ultrasonic buffer technique⁹ to determine wave velocities in the frequency range of 60 - 500 Mc. From these the elastic moduli of the crystals are calculated (Table 1). Solbrig¹⁰ used crystals fabricated by the same method as piezoelectric resonators and calculated these constants from the resonant frequencies. Hemphill¹¹ measured the attenuation of ultrasound in ZnO using the pulse-echo method and found that the attenuation depends exponentially on frequency with an exponent of 1.62 for longitudinal waves propagating parallel to the c-axis. He reports a value of 14 db/cm attenuation at 1GHz at room temperature in a lithium compensated crystal of $10^{12} \Omega\text{-cm}$ resistivity. Hutson¹² and Hemphill report values for the electromechanical coupling constant K_{33} , of single crystals, between 0.3 and 0.4, while recently a value of 0.48 has been measured³².

PROPERTIES OF ZINC OXIDE

PROPERTY	VALUE	REF.
Lattice Const.	$a = 3.25 \text{ \AA} , c = 5.19 \text{ \AA} , c/a = 1.60$	(13)
Distance of Neighbouring Ions	to c-axis : $d = uc = 1.96 \text{ \AA} , u = 0.378 ,$ for others : $d = \sqrt{(a^2/3) + c^2(u - 1/2)^2} = 1.98 \text{ \AA}$	(13)
Molecular Weight & Density	Zn : 65.38 ; O : 16.00 ; ZnO : 81.38 $5.62 - 5.78 \text{ g/cm}^3 \rightarrow 4.21 \text{ molecules/cm}^3$	(13)
Elastic Constants	$C_{11}^E \quad C_{12}^E \quad C_{13}^E \quad C_{33}^E \quad C_{44}^E \quad C_{66}^E$ $\times 10^{10} \text{ N/m}^2$ (8)	&
	21.0 12.1 10.5 21.1 4.25 4.43	
Elastic Constants	$S_{11}^E \quad S_{12}^E \quad S_{13}^E \quad S_{33}^E \quad S_{44}^E \quad S_{66}^E$ $\times 10^{12} \text{ m}^2/\text{N}$ (37)	
	7.86 -3.43 -2.21 6.94 2.36 2.26	
Sound Velocity	$V_l \parallel c = 6.0961 \times 10^5 \text{ cm/sec} ; V_l \perp c = 6.0776 \times 10^5 \text{ cm/sec}$ $V_s \parallel c = 2.7353 \times 10^5 ; V_s \perp c = 2.7350 \times 10^5$	(8)
Piezoelectric Constant	$e_{15} = -0.59 \text{ c/m}^2 , d_{15} = -13.9 \times 10^{-12} \text{ c/N}$ $e_{31} = -0.61 \text{ c/m}^2 , d_{31} = -5.2 \times 10^{-12} \text{ c/N}$ $e_{33} = 1.14 \text{ c/m}^2 , d_{33} = 10.6 \times 10^{-12} \text{ c/N}$	(37)
Dielectric Constants	$\epsilon_{33}^T = 11.0X \epsilon_o , \epsilon_{33}^S = 8.84 \times \epsilon_o$ $\epsilon_{11}^T = 9.26X \epsilon_o , \epsilon_4^S = 8.33 \times \epsilon_o$	(37)
Refr. Index	$\eta_c = 2.0$ for single cryst. $\eta_c = 1.57$ for porous thin film	(15)
Enthalpy of Formation	Zn (solid) + 1/2 O ₂ (gas) → ZnO (solid) : - 83.17 K cal/mole lattice energy : 965 K cal/mole	(13)
Melting Point	T _m = 1800 - 2000°C at atmospheric pressure	(13)
Vapour pressure	12 torr at 1500°C ; sublimation appreciable in vacuum at 1000°C	(13)
Energy Gap	E _g = 3.2 - 3.35 eV (at 0°K)	(14)
Eff. carrier mass	$m^*/m = 0.32$	(12)
	$= 0.38$	(16)
	$= 0.14$	(14)

CHAPTER III

ANALYSIS OF TRANSDUCER PERFORMANCE

3.1 Introduction

A theoretical analysis of the piezoelectric transducer is presented in this section, resulting in an equivalent circuit representation and an insertion loss vs. frequency characteristic for the specific loading conditions used in this experiment.

The choice of starting equations, leading to the required equivalent circuit in the most straightforward manner, depends on the shape of the transducer and on the experimental conditions. All devices considered here are of the thin disk form with plane-parallel electrodes placed perpendicular to the smallest dimension of the disc, producing an electric field that is parallel to the propagation of the induced longitudinal bulkwaves. The surface dimensions of the device are orders of magnitude larger than its thickness, and in the following analysis it is assumed that all points in any given plane parallel to the electrodes are moving with equal displacements and there exists no phase difference from point to point. This reduces the problem to one dimension. The transducer is loaded on one face with a mechanical load (substrate) while the other face is free. The free-face assumption is permitted by the fact, that the thickness of the applied electrodes is less, than $1/4$ wavelength of the mechanical vibrations. The set of thermodynamic equations describing a system acted upon by electric and mechanical fields under adiabatic conditions, with strain and charge density chosen as the independent variables (as suggested by the physical setup, since the strain is one-dimensional, and for at least one of the cases considered the charge density is nonspacevariant) is as follows :

$$T = c^D S - h D \quad (1)$$

$$E = -h S + \beta D \quad (2)$$

where D is the electric displacement, E the electric field, T the stress and S the strain.

The constants are defined as :³

$$h = (-\partial E / \partial S)_D = (d c^E) / e^S ; \quad s = \partial l / \partial x ;$$

$$d = (\partial D / \partial T)_E = (\partial S / \partial E)_T ;$$

$$e^S = (\partial D / \partial E)_s = e^T - c^E d^2 ; \quad e^T = (\partial D / \partial E)_T ;$$

$$c^D = (\partial T / \partial S)_D = e^T (c^E / e^S) ; \quad c^E = (\partial T / \partial S)_E ;$$

$$c^D = (e^T c^E) / (e^T - c^E d^2) ; \quad \beta = (1 / e^S) .$$

We shall consider two main cases, that of the perfect dielectric and that of the semi-conductive transducer (extrinsic), and in both cases we assume the nonexistence of surface waves and current leakage on the surfaces.

3.2 The Perfect Dielectric Transducer

Calculations here are greatly simplified by the fact⁰ that

$$\nabla \cdot D = 0 .$$

According to Newton's law

$$\left(\frac{\partial T}{\partial x} \right) = \rho \left(\frac{\partial^2 l}{\partial t^2} \right) \quad (3)$$

with ρ being the mass density and l the mechanical displacement. Substituting from Equation (1) and (2) into Equation (3), while taking into account the zero conductivity and assuming harmonic excitation of the form $l = l_0 \exp j\omega t$, this becomes :

$$\left(\frac{d^2 l}{dx^2} \right) + k^2 l = 0 \quad (4)$$

where

$$k = \omega / v^D$$

and

$$v^D = (c^D / \rho)^{1/2}$$

The general solution of Equation (4) is

$$l = A \sin kx + B \cos kx \quad (5)$$

where x is the direction of longitudinal wave propagation; v^D is the wave velocity; ω the angular frequency and k is the propagation constant. Let the forces F_1 and F_2 act on the faces of the transducer at $x = 0$ and $x = L$ respectively. According to the sign convention compressional forces are negative and thus if A is the area of the transducer, then :

$$F(x)/A = -T(x); \quad v_1 = \left(\frac{\partial l}{\partial t} \right)_{x=0} ; \quad v_2 = \left(-\frac{\partial l}{\partial t} \right)_{x=L}$$

for compression. Substituting into Equation (5) :

$$v_1 = j\omega B ; \quad B = (v_1 / j\omega)$$

$$v_2 = -j\omega [A \sin kL + (v_1 / j\omega) \cos kL]$$

$$A \sin kL = -v_2/j\omega - (v_1/j\omega) \cos kL$$

$$I = (1/j\omega) \left\{ \left[-v_1/\tan kL - v_2/\sin kL \right] \sin kx + v_1 \cos kx \right\} \quad (6)$$

Thus from Equation (1) :

$$F_1/A = (hD - c^D \partial I / \partial x)_{x=0} \quad)$$

$$F_2/A = (hD - c^D \partial I / \partial x)_{x=L} \quad)$$

and if I is the impressed sinusoidal external current, then

$$D = I/j\omega A$$

This results in the equations

$$F_1/A = hI/j\omega A + (k c^D/j\omega) \left[v_1/\tan kL + v_2/\sin kL \right] \quad (7)$$

$$F_2/A = hI/j\omega A + (k c^D/j\omega) \left[v_1/\sin kL + v_2/\tan kL \right] \quad .$$

Also

$$V = \int_0^L E dx = \int_0^L (\beta D - h \partial I / \partial x) dx \quad , \quad (8)$$

$$V = \beta LI/j\omega A + (h/j\omega) (v_1 + v_2) \quad .$$

Defining $Z_0 = (c^D/v^D)$ as the characteristic impedance of the material, the set of equations describing the behaviour of the transducer is :

$$F_1 = (Z_o A / j \tan kL) v_1 + (Z_o A / j \sin kL) v_2 + hI / j\omega$$

$$F_2 = (Z_o A / j \sin kL) v_1 + (Z_o A / j \tan kL) v_2 + hI / j\omega \quad (9)$$

$$V = (h/j\omega) v_1 + (h/j\omega) v_2 + \beta LI / j\omega$$

These equations can be represented by a three-port electromechanical model, incorporating an ideal transformer with turns ratio defined by :

$$N = (\text{force out} / \text{voltage in})_{s=0} = (hA/\beta L)$$

and containing at least four impedances, corresponding to the four distinct coefficients in Equation (9). This model is shown in Figure 3a. By setting up loop equations for this circuit one obtains :

$$F_1/N = (Z_1 + Z_i + Z_e) v_1 N + (Z_i + Z_e) v_2 N + Z_e I$$

$$F_2/N = (Z_i + Z_e) v_1 N + (Z_2 + Z_i + Z_e) v_2 N + Z_e I \quad (10)$$

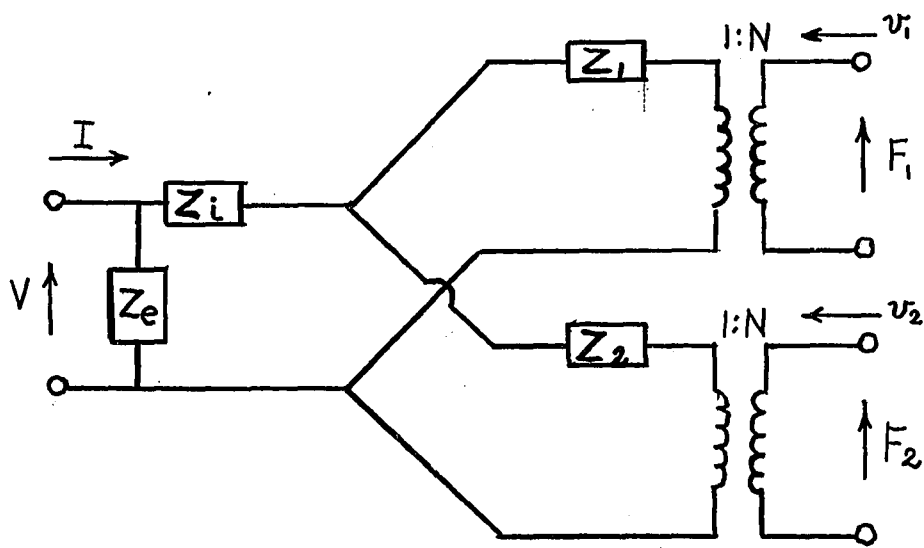
$$V = Z_e v_1 N + Z_e v_2 N + Z_e I$$

The impedance values are now arrived at by equating the coefficients of sets (9) and (10) :

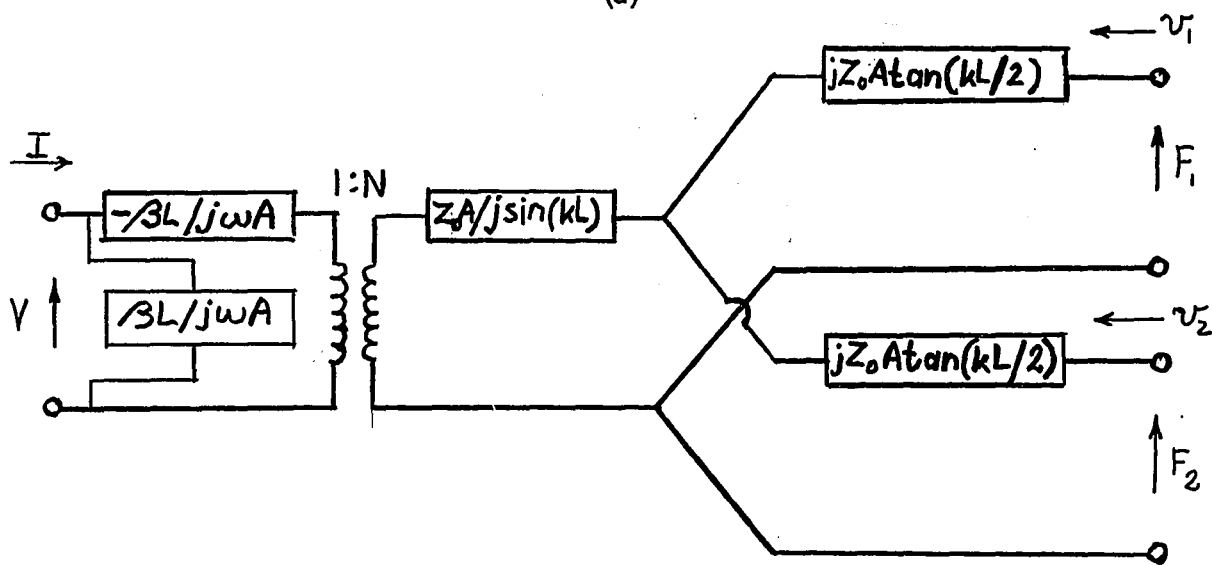
$$Z_e = \beta L / j\omega A$$

$$Z_i = (Z_o A / N^2 j \sin kL) - (\beta L / j\omega A)$$

$$Z_1 = Z_2 = j(Z_o A / N^2) \tan (kL/2)$$



(a)



(b)

Figure 3 - Electromechanical Model of Dielectric Piezoelectric Transducer.

(a) General Circuit

(b) Actual Model with Impedance Values Shown.

These impedances are shown in the slightly modified model of Figure 3b.

3.3 Extrinsic Semiconductor Transducer

The physical setup remains the same as in the previous case and the semiconductor is taken to be of the p-type. For n-type semiconductors the analysis differs only in the appropriate signs. As opposed to the dielectric case, we are dealing with a finite space-varying conductivity and space charge density. This necessitates the derivation of a relation between the electric field and electric displacement in order to be able to make use of the thermodynamic equations of state. The notation used is :

$$\begin{aligned} E &= E_0 + E_1 & , & & D &= D_0 + D_1 & , \\ \mathcal{G} &= \mathcal{G}_0 + \mathcal{G}_1 & , & & p &= p_0 + p_1 & , \end{aligned}$$

where : E_0 and D_0 are the time-varying, steady state, non-space-dependent, components of the electric field and electric displacement. \mathcal{G}_0 and p_0 are the non-space-dependent components of the conductivity and carrier density respectively; while E_1 , D_1 , \mathcal{G}_1 , p_1 , are the instantaneous space-dependent components of the same variables. The derivation is based on the assumption, that the nonlinear terms in the system are negligible.

The current density in the transducer bulk is given by :

$$J_{int} = uq(p_0 + p_1)(E_0 + E_1) - \cancel{(k_0 T_0)} (\partial p / \partial x) ,$$

where u is the mobility, k_0 is the Boltzman constant and T_0 is the temperature.

$$\begin{aligned} \nabla \cdot J_{\text{int}} = & uqE_0 (\partial p_1 / \partial x) + uqp_0 (\partial E_1 / \partial x) + uqE_1 (\partial p_1 / \partial x) + \\ & + uqp_1 (\partial E_1 / \partial x) - (uk_0 T_0) (\partial^2 p_1 / \partial x^2) . \end{aligned} \quad (11)$$

From Poisson's equation and the continuity equation

$$(\partial D / \partial x) = (\partial D_1 / \partial x) = qp_1 , \quad \nabla \cdot J_{\text{int}} = - \partial (qp_1) / \partial t , \quad (12)$$

and thus

$$\begin{aligned} (- \partial^2 D_1 / \partial t \partial x) = & uE_0 (\partial^2 D_1 / \partial x^2) + uqp_0 (\partial E_1 / \partial x) + u (\partial D_1 / \partial x) (\partial E_1 / \partial x) \\ & + uE_1 (\partial^2 D_1 / \partial x^2) - (uk_0 T_0 / q) (\partial^3 D_1 / \partial x^3) . \end{aligned} \quad (13)$$

From the thermodynamic equations of state, equations (1) and (2), and from Newton's law, equation (3),

$$\begin{aligned} (\partial E_1 / \partial x) &= -h (\partial^2 I / \partial x^2) + \beta (\partial D_1 / \partial x) , \\ (\partial T / \partial x) &= c (\partial^2 I / \partial x^2) - h (\partial D_1 / \partial x) , \\ (\partial T / \partial x) &= \mathcal{F} (\partial^2 I / \partial t^2) . \end{aligned}$$

From this it follows that,

$$(\partial D_1 / \partial x) = (c/h) (\partial^2 I / \partial x^2) - (\mathcal{F}/h) (\partial^2 I / \partial t^2) . \quad (14)$$

Substituting Equation (14) into (13) and deleting nonlinear terms from the resulting expression, one obtains the following linear differential equation for l :

$$\begin{aligned}
 & (-c/h) (\partial^3 l / \partial t \partial x^2) + (-\mathcal{F}/h) (\partial^3 l / \partial t^3) = \\
 & (u q p_o / h) [(\beta c - h^2) (\partial^2 l / \partial x^2) - \beta \mathcal{F} (\partial^2 l / \partial t^2)] \\
 & - (u k_o T_o / q h) [c (\partial^4 l / \partial x^4) - \mathcal{F} (\partial^4 l / \partial x^2 \partial t^2)] .
 \end{aligned} \tag{15}$$

The above is satisfied by a solution of the general form

$$l = l_o e^{i(kx + \omega t)} ,$$

with similar representation for D and E , and by making use of this an equation in k , the propagation constant, is obtained.

$$\begin{aligned}
 k^4 (c^D u k_o T_o / q) + k^2 (u q p_o \beta c^D - u q p_o h^2 - u k_o T_o \mathcal{F} \omega^2 / q + j \omega c^D) + \\
 (j \mathcal{F} \omega^3 - u q p_o \beta \mathcal{F} \omega^2) = 0 .
 \end{aligned} \tag{16}$$

Equation (16) gives four distinct values for k upon solution. Two of these values represent acoustic waves and the other two carrier waves³⁰. Here the assumption is made that for the frequencies of interest the effect of the carrier waves is negligible, and the acoustic propagation constant is given by

$$(k/\omega) \approx (v^D)^{-1} = \text{constant} .$$

Defining

$$u k_o T_o k^2 / q \omega^2 = 1 / \omega_D ,$$

and recalling that

$$\mathcal{G} \approx \mathcal{G}_o = u q p_o ,$$

equation (16) is modified as follows :

$$k^2 = \mathcal{G} \omega^2 \left[\mathcal{G} \beta + (\omega^2 / \omega_D) + i \omega \right] / \left[(\omega^2 c^D / \omega_D) + \mathcal{G} (\beta c^D - h^2) + i c^D \omega \right] .$$

(17)

From equation (17) k is found in terms of the physical constants of the material, but the values are only approximate because the carrier waves were neglected. We are now in the position to find the displacement as a function of the face-velocities of the transducer. The details of this calculation are omitted since the steps parallel those of the dielectric case. The result is :

$$l = (1 / i \omega) \left[(-v_1 / \tan kL - v_2 / \sin kL) \sin kx + v_1 \cos kx \right] .$$

(18)

As in the dielectric case

$$F_1 / A = \left[h D - c^D (\partial l / \partial x) \right]_{x=0}$$

$$\left[c^D (\partial l / \partial x) \right]_{x=0} = (-c^D k / i \omega) (v_1 / \tan kL + v_2 / \sin kL) .$$

In order to evaluate $(h D)_{x=0}$, consider the following :

$$J_{\text{external}} = J_{\text{conduction}} + J_{\text{diffusion}} + J_{\text{displacement}}$$

$$J_{\text{ext}} = \epsilon_0 E - (u k_0 T_0 / q) (\partial^2 D_1 / \partial x^2) + j \omega D .$$

The last term in the above is a result of the fact that D and E must have the same wave-form as the displacement, as is evident from equation (14). From equation (13) a simple relationship between E_1 and D_1 can be obtained as follows :

$$-k \omega D_1 = -k^2 u E_0 D_1 - j k \epsilon_0 E_1 - j k^2 u E_1 D_1 - k^2 u E_1 D_1 - (u k_0 T_0 / q) j k^3 D_1 . \quad (19)$$

Deleting nonlinear terms and rearranging the above while making use of the definition for ω_D one gets :

$$D_1 = (j \epsilon_0 / \omega) / (1 - j \omega / \omega_D) E_1$$

$$D_1 = M E_1 .$$

Therefore

$$E = E_0 + E_1 = D_0 / \epsilon^s + D_1 / M . \quad (20)$$

The external current cannot be space-varying, hence the space-varying portions of all internal current contributions must balance out to zero, which permits separate handling of the time-varying and space-varying parts of the current densities.

$$J_{\text{ext}} = I/A = j\omega D_o + (\sigma_o/e^s) D_o$$

$$D_o = I/(j\omega + \sigma_o/e^s) A \quad (21)$$

$$D = D_1 + D_o = D_1 + I/RA, \quad R = (j\omega + \sigma_o/e^s),$$

and since from equation (2)

$$D_1 = [Mh/(M\beta - 1)](\partial I/\partial x),$$

it follows that

$$D_{x=0} = [(-k/j\omega)Mh/(M\beta - 1)](v_1/\tan kL + v_2/\sin kL) + I/RA,$$

$$D_{x=L} = [(-k/j\omega)Mh/(M\beta - 1)](v_1/\sin kL + v_2/\tan kL) + I/RA.$$

(22)

From equation (22) the expression for the force F_1 is written as :

$$F_1/A = [h^2 k M/(1 - M\beta) + c^D k] (1/j\omega) (v_1/\tan kL + v_2/\sin kL) + (h/RA)I,$$

and the equation for F_2 is arrived at similarly. The terminal voltage V is given by :

$$V = \int_0^L E dx = \int_0^L [-h(\partial I/\partial x) + \beta D] dx,$$

$$V = \int_0^L [-h + \beta Mh/(M\beta - 1)] (\partial I/\partial x) dx + (\beta/RA)I dx,$$

$$V = [h/(M\beta - 1)] [I]_0^L + (\beta L/RA)I,$$

$$V = (-1/j\omega) [h/(M\beta - 1)] (v_1 + v_2) + (\beta L/RA) I.$$

Now let

$$G = (-1/j\omega) [h/(M\beta - 1)] ,$$

$$Z_o = h^2 kM/\omega(1-M\beta) + c^D k/\omega ,$$

(note that Z_o here is different from that in the dielectric case and the same symbol is used only in order to point out the similarity in the form of the following equations) and then :

$$F_1 = (Z_o A/j \tan kL) v_1 + (Z_o A/j \sin kL) v_2 + hI/R$$

$$F_2 = (Z_o A/j \sin kL) v_1 + (Z_o A/j \tan kL) v_2 + hI/R \quad (23)$$

$$V = G v_1 + G v_2 + (\beta L/RA) I .$$

The coefficient matrix of set (23) is not symmetrical and a model based on it will not be reciprocal in its behaviour. This again is the result of having neglected carrier waves, but at the same time having retained the effect of diffusion on the acoustic waves. These effects are contained in the expression for M :

$$M = (j\sigma_o/\omega)/(1-j\omega/\omega_D) \quad \rightarrow \quad (j\sigma/\omega)$$

as $\omega_D \rightarrow \infty$.

(Recall that $1/\omega_D \propto D_i$; where D_i is the diffusion constant). In this case :

$$G' = h/j\omega (1 - j\sigma\beta/\omega) = h/R ,$$

$$Z_o' = h^2 k (j\sigma\beta/\omega)/(1 - j\sigma\beta/\omega) + c^D k/\omega ,$$

and the resulting set of equations is symmetrical. Computations show, that efficiency figures arrived at on the basis of these two approximations vary by less than one percent up to a conductivity of 10^{-4} ohm meters. The models in Figure 4 are based on equation (23). Defining an ideal transformer as before :

$$N = h A / \beta L ,$$

the loop equations for Figure 4a are as follows :

$$\begin{aligned} F_1 &= (Z_1 + Z_i + Z_e) N^2 v_1 + (Z_e + Z_i) N^2 v_2 + N B I \\ F_2 &= (Z_i + Z_e) N^2 v_1 + (Z_2 + Z_i + Z_e) N^2 v_2 + N B I \\ V &= G N v_1 + G N v_2 + Z_e I. \end{aligned} \quad (24)$$

Equating coefficients of equations (23) and (24), the impedance values are obtained.

$$Z_e = \beta L / RA , \quad Z_1 = Z_2 = j Z_o A / N^2 \tan (kL / 2) ,$$

$$Z_i = (Z_o A / N^2 j \sin kL) - (\beta L / RA) .$$

3.4 Insertion Loss Calculations

Figure 4b is the actual model of the transducer loaded with a mechanical load Z_L on one face and free on the other. Using current directions indicated on the diagram :

$$V = - G i_2 + I Z_e = - G i_2 + I B ,$$

$$N V = N B I = i_2 (Z_b + Z_T) - i_3 Z_T ,$$

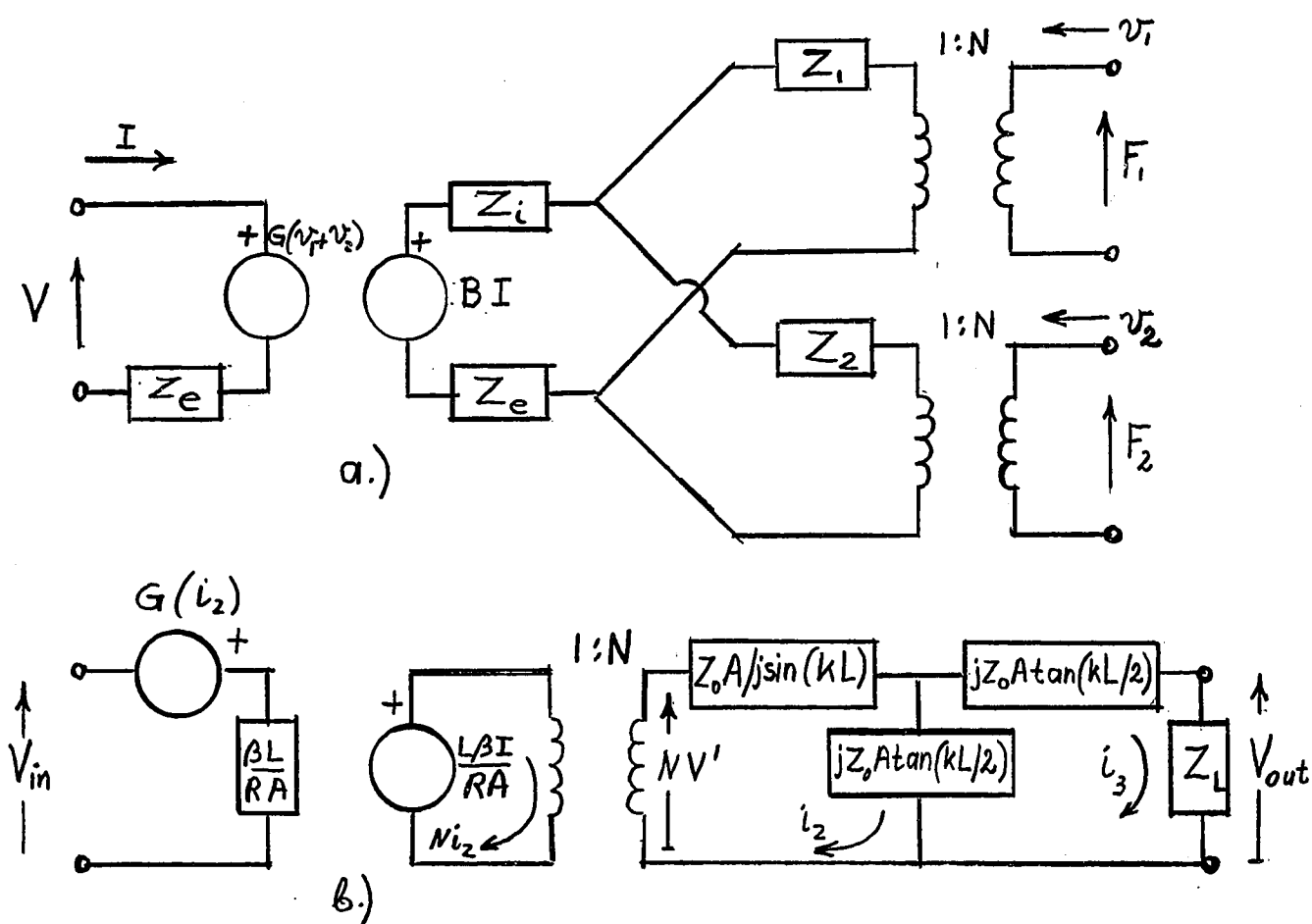


Figure 4 - Electrical Equivalent Circuit of Semiconducting Transducer.

where $Z_T = N^2 Z_1$ and $Z_b = N^2 (Z_i + Z_e)$.

$$Z_T i_2 = (Z_L + 2 Z_T) i_3 ,$$

$$N B I = i_3 \left[\frac{(Z_b + Z_T)(Z_L + 2 Z_T)}{Z_T} - Z_T \right] ,$$

$$V_{out} = i_3 Z_L = I N B Z_L Z_T / \left[(Z_b + Z_T)(Z_L + 2 Z_T) - (Z_T)^2 \right] ,$$

$$Z_{in} = B - G N B (Z_L + 2 Z_T) / \left[(Z_b + Z_T)(Z_L + 2 Z_T) - (Z_T)^2 \right] ,$$

$$V_{in} = I Z_{in} ,$$

$$\eta_{EM} = P_o / P_{in} = (|V_o|^2 / |V_i|^2) (Re Y_L / Re Y_{in}) ,$$

where η_{EM} is the electrical - to - mechanical conversion efficiency.

If the delay line to which power is delivered is assumed lossless and if all the power is reflected from its other end back to the transducer, then the insertion loss of the device will depend only on the conductivity and on the matching conditions. Let the transmission coefficient at the generator - transducer terminals be T_1 and at the delay line-transducer terminals be T_2 , then :

$$T_1 = 1 - |(Z_s - Z_{in})^2 / (Z_s + Z_{in})^2| ,$$

$$T_2 = 1 - |(Z_R - Z_L)^2 / (Z_R + Z_L)^2| ,$$

where Z_s is the impedance of the generator and Z_R is the impedance seen by the delay line, including any terminations (tuning network, generator) connected across the electrical end of the transducer. If the mechanical - to - electrical conversion efficiency is η_{ME} , then the insertion loss is defined by :

$$IL = \text{conversion loss} + \text{transmission loss},$$

$$IL = 10 \log (\eta_{EM} \times \eta_{ME}) + 10 \log (T_1 \times T_2) \text{ decibels.}$$

3.5 Results of Computations

There are three often used electrical terminations for transducers :

- a.) "continuous tuning", meaning that there is a tuning network inserted between the generator and the transducer, and is adjusted at all frequencies of measurement for maximum power transfer (i.e. : the transducer has the complex conjugate of its input impedance connected across its electrical terminals),

b.) the area of the acoustic beam (the area of the top electrode) is adjusted so as to make the clamped input reactance of the transducer numerically equal to Z_s at the frequency for which the length of the transducer is a half wavelength of the sound wave,

c.) a fixed inductor is inserted across the electrical terminals of the transducer, of such value that it tunes out the input capacitance at the half-wavelength-frequency.

Figure 5 shows the results of conversion loss computations for a continuously tuned ZnO transducer on a sapphire delay line and half-wavelength-frequency of one gigahertz. Electro-mechanical conversion loss is higher than the mechanical-electrical one for both of the plotted conductivities (10^{-2} and $10^{-1} \Omega \text{ m}$), which is due to better matching at the generator end. The sapphire and the tuning network have been assumed lossless and conversion loss, rather than insertion loss, has been plotted because in the case of continuous matching this is the dominant term.

The insertion losses of an untuned and an inductively tuned (cases b and c) transducer are compared in Figure 6. Inductive tuning reduces the loss by about 30 db and gives a greater bandwidth than no tuning, but the minimum loss is 3.33 db (dielectric), while for continuous tuning it is zero. Because the transmission loss is the dominant factor here, there is only 2 - 4 db difference in the loss of the dielectric transducer and of one with $10^{-1} \Omega \text{ cm}$ conductivity near the half wavelength frequency.

For all three types of tuning, the computations show, that a transducer having a conductivity lower than $10^{-4} \Omega \text{ m}$ may be considered dielectric with an error of less than 0.01 db. The physical constants in all calculation were those given in reference 37.

Figure 5 - Conversion Loss of Continuously Tuned Transducer.

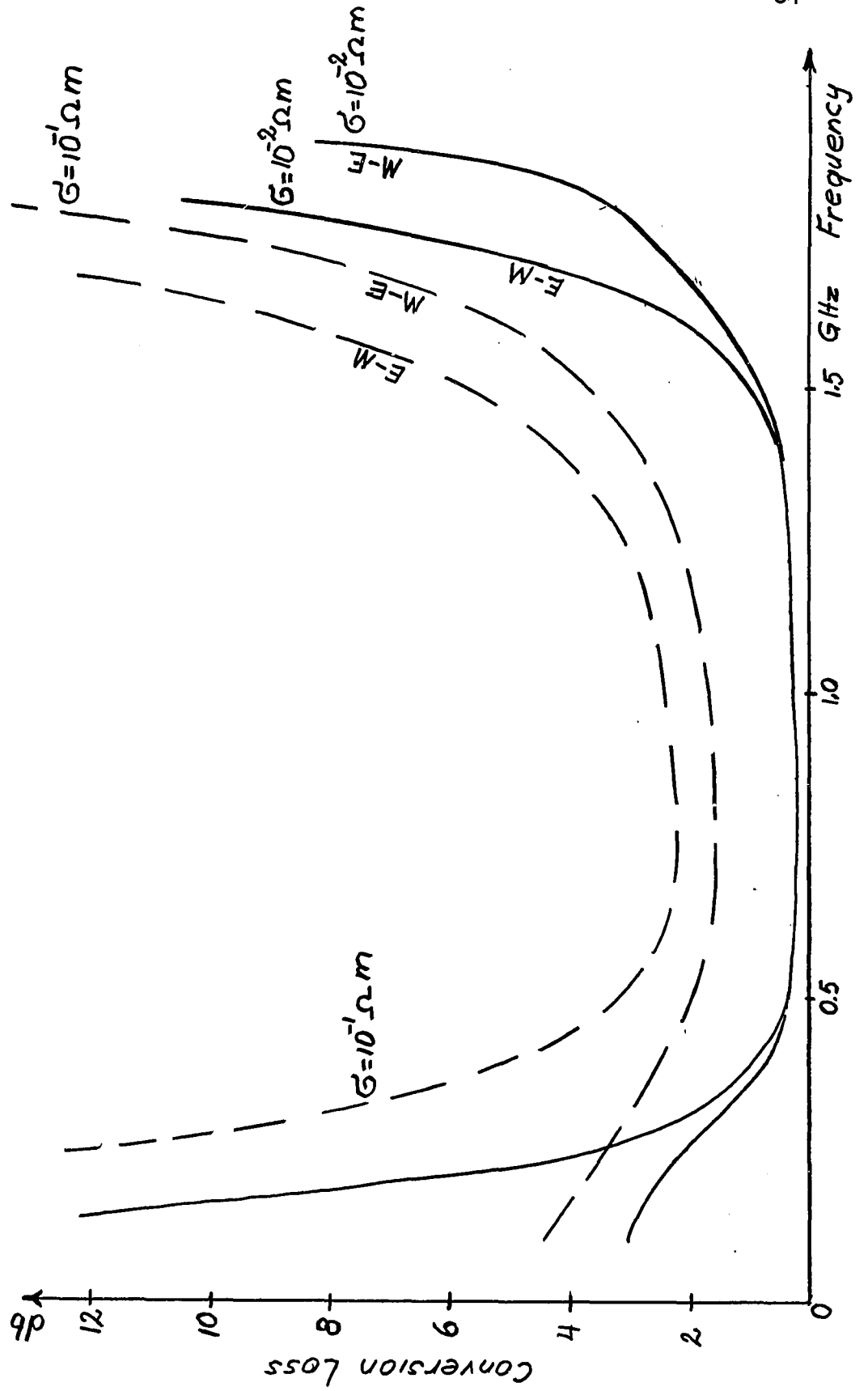
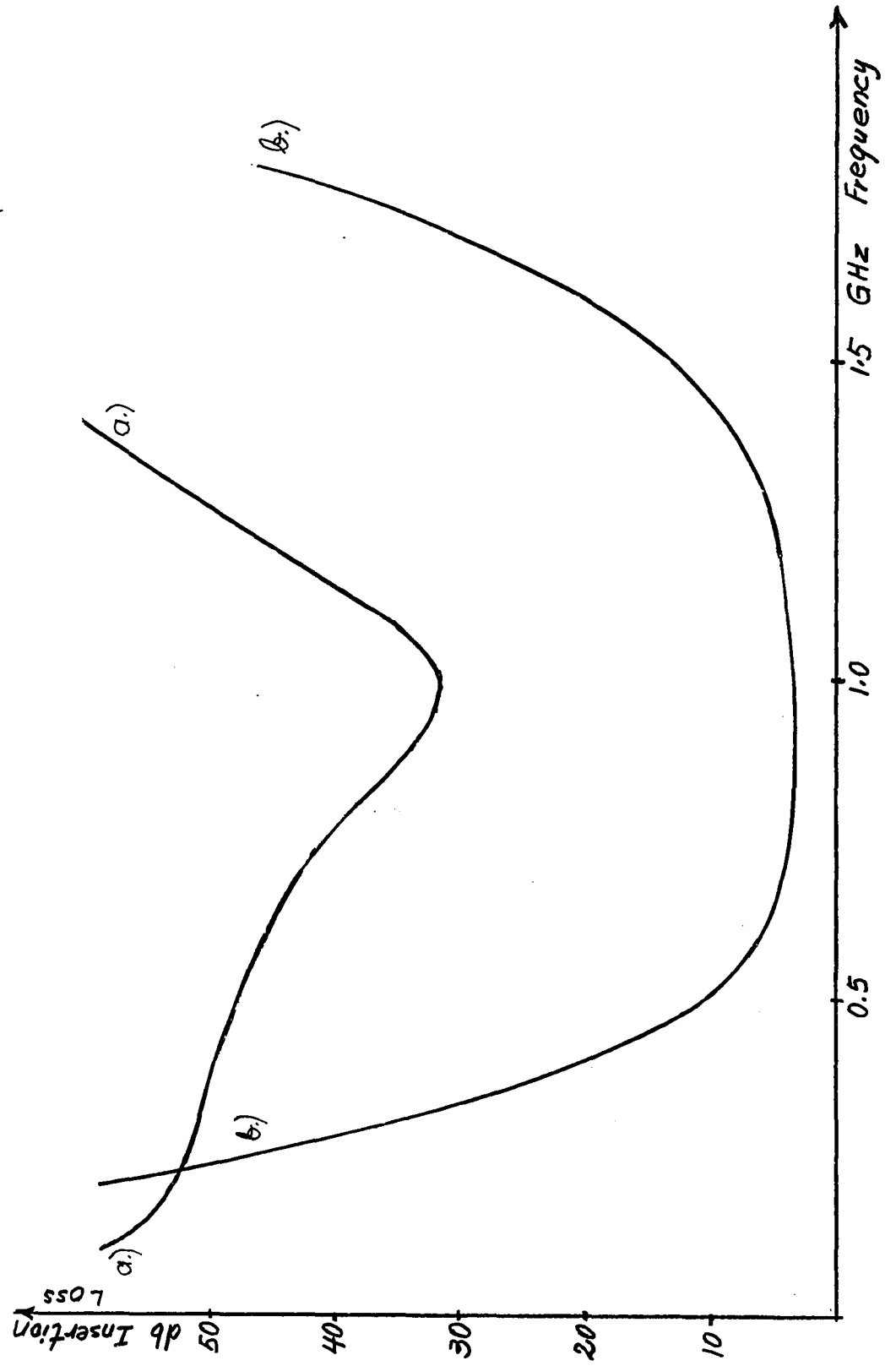


Figure 6 - Insertion Loss of Untuned and of Inductively Tuned Transducer.

(a) No Tuning (b) Inductive Tuning



CHAPTER IV

METHODS OF DEPOSITION

4.1 Introduction

In this experiment the first harmonic of the transducer to be manufactured was in the 1-2 gigahertz range corresponding to a film of thickness of 1-4 microns. To this end one could have conceivably grown a plate-like crystal out of a liquid solution of ZnO and affix it to a suitable delay line with a resin or cement and then proceed to polish down the plate until the desired thickness is reached. The polishing and cementing procedures are however very difficult to carry out with sufficient parallelism and smoothness and there are considerable losses in the resin.

Direct growing of the ZnO film on the substrate is a more convenient method. Evaporation is difficult, due to decomposition, as discussed in Chapter II. Deposition and subsequent oxidation of zinc films is possible, but the results are of poor uniformity and one cannot predict what the orientation is going to be. Evaporation of zinc in the presence of oxygen is a workable method but substrate temperatures are extremely critical and adhesion to the substrate leaves much to be desired.

Sputtering has been used successfully by Foster³⁶ to prepare ZnO transducers out of ZnO cathode sources and, because of the many inherent advantages of sputtering over evaporation, this method was chosen here. These advantages are :

- (a) low temperature of source material,
- (b) high vacuum is not essential,
- (c) adhesion is better,
- (d) compounds are deposited without decomposition

- (e) films are of high uniformity,
- (f) film thickness is linearly dependent on time of

deposition. The main disadvantages are higher impurity concentration, slower deposition and the greater complexity of the needed apparatus.

4.2 Glow Discharge

Sputtering is defined as the disintegration of a cathode under ionic bombardment in an electric glow discharge in a low-pressure gas. The phenomenon is observed in the 1-100 millitorr pressure range.

If two electrodes are immersed in a low pressure gas and a sufficiently high voltage is impressed across them a current will flow due to the ionization of the gas in the intervening space. The ionized gas emits a glow, the colour of which is typical of the gas(es) present. The voltage at which discharge is struck is usually lower than the theoretical potential necessary for dielectric breakdown because of the presence of free electrons in the vacuum and because of the thermally assisted field emission of electrons from the electrode surfaces. These electrons are accelerated in the interelectrode space and ionize the gas by collision. Once the discharge is struck, the voltage necessary for its maintenance is even lower than previously because of the increased number of electrons, provided partially by the ionization process itself and partially by the more efficient emission from the cathode due to ionic bombardment.

The mobility of the electrons in the gas is higher than that of the ions and as a result they reach the anode before the ions reach the cathode. Visual evidence of this is a strongly glowing "positive column" near the anode. Separating the cathode from this anode glow is a well defined "dark space" the length of which is dependent on the ioniza-

tion energy of the gas and on the probability of a collision between electrons and gas molecules. A reduction in the gas pressure reduces this probability, thus reducing the ionization efficiency and the current flowing, and increases the length of the dark space. If the gas pressure is reduced until the dark space reaches the anode, the discharge is extinguished.

When the minimum voltage necessary for a stable discharge is reached the glow is said to be "normal". At this point the glow covers only part of the cathode surface. Increasing the current expands the glow at a constant voltage until the entire cathode area is covered. Beyond this point increases in current are only possible by increases in current density and a correspondingly higher voltage. This rising part of the V-I characteristic is termed as "abnormal glow" and is the part of main interest from the point of view of physical sputtering. Beyond a critical voltage, determined by cathode area, shape, material, gas pressure, etc., the glow degenerates into an arc discharge, (see Figure 7).

The mean free path of a particle in the plasma is of critical importance in the design of sputtering equipment, partly because of ionization efficiency and partly because of the dependence of film-to-substrate adhesion on the arriving particle energy, which in turn depends on the number (and kind) of collisions it suffers on the way from the cathode to the substrate. The mean free path is given by

$$l = 1 / (2\pi n^2 \sigma),$$

where n is the number of colliding particles per unit volume, σ is the collision diameter. For constant temperature n is proportional to the pressure P and thus for a given gas composition $l = A/P$ where A is a constant. This relationship however is complicated by the

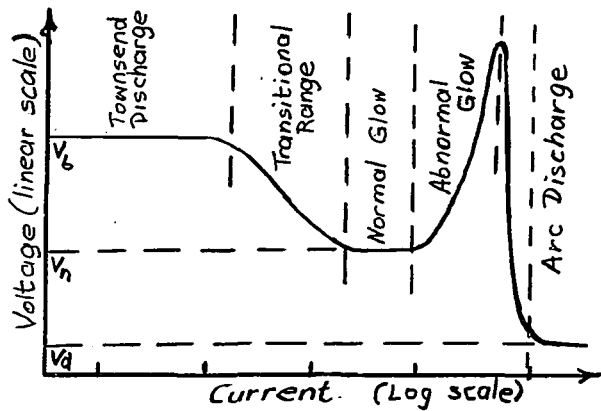


Figure 7 - V-I Characteristic of Glow Discharge

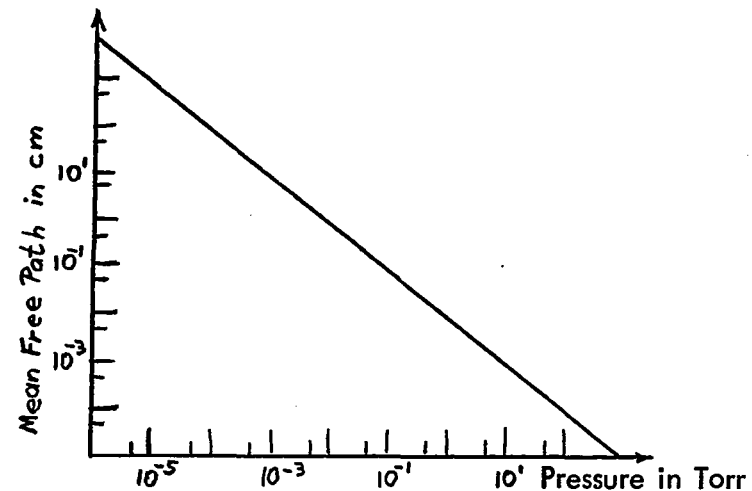


Figure 8 - Mean Free Path in Argon

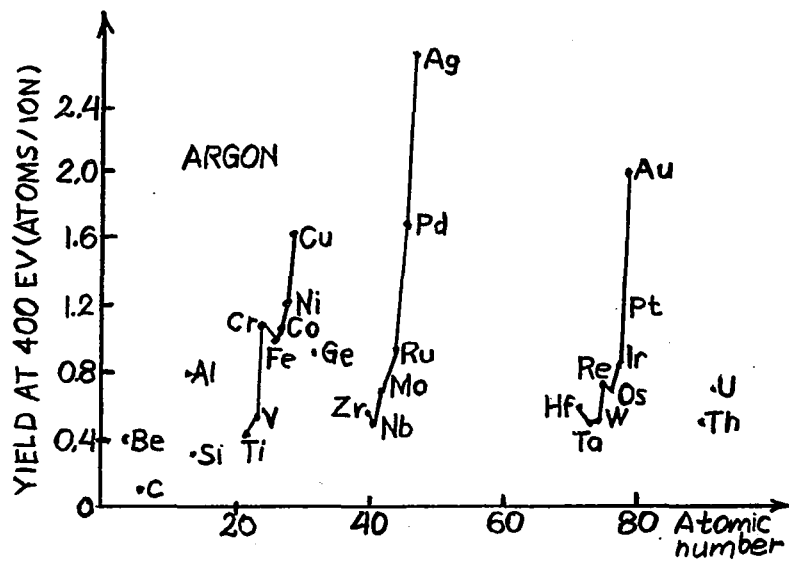


Figure 9 - Yield as a Function of Atomic Number in Argon¹⁸

difficulty in defining what one means by plasma temperature and how to keep it constant independently of pressure? Temperature is a function of the mean translational kinetic energy of the particles and of other modes of energy storage and these in turn vary from place to place in the plasma and are different for the different constituents. Since the mean kinetic energy is a function of the number of collisions, it is also a function of pressure. Figure 4 shows the plot of mean free path vs. pressure in an argon discharge. This plot is particularly useful since argon is the gas most often used in physical sputtering.

4.3 Sputtering Mechanisms

Currently there are three main theories explaining the process of sputtering. None of them is applicable to all experimental facts and the total process is probably due to a combination of all mechanisms described below :

(a) "Chemical sputtering" refers to the formation of compounds on the cathode surface which are volatile at the surface temperature. These compounds are created by a chemical reaction between residual gases in the system and the cathode material. This mechanism is characterized by a constant yield independent of ion energy and does not account for the sputtering of non volatile matter. It is important only at low ion energies and in "unclean" systems, where a continuous out-gassing of the walls and fixtures provides the necessary gases for the reaction.¹⁸

(b) The creation of localized hot spots is thought to be due to a transfer of the bombarding ion's energy to one or more of the surface molecules in a nondirectional manner, increasing their thermal motion and causing them to escape. Evaporation is a similar process, but here the escape takes place before appreciable amounts of energy could

be transferred to deeper layers and the bulk remains cool. "Hot spot" theory predicts a spacial distribution of the deposit according to cosine law and independence from the angle of incidence of the ion beam. The yield of sputtered material per incident ion, S , is then linearly dependent on the ion energy V_i :

$$S = a (V_i - V_o) ,$$

where a and V_o are constants determined by the particular make-up of the system. This mechanism is of importance in the mid-range of ion energies¹⁹⁻²¹.

(c) "Physical sputtering" is predominant in the lower and probably in the upper ion energy ranges. The ion energy is of prime interest, because of the depth of penetration determined by it. At high energies the ion interacts with the molecules of the cathode through coulombic repulsion of the nuclei. In the mid-range the electron cloud partially obscures the effect of this repulsion and a mixed electro-mechanical collision takes place. At low energies there is very little penetration of the electron shell and a classical hard-sphere collision occurs. The ranges are : low 0.5-5 Kev, mid 5-10 Kev, high 10-50 Kev. Most of the thin film work is carried out in the low mid-range and the mechanical hard-sphere collision or physical sputtering theory is the most significant of the three. This theory assumes that momentum is transferred to the surface molecules of the cathode in one of two modes :

- a.) The incident ion passes through the top layer and is reflected by a lower lying molecule and on its way out dislodges a surface particle,

- b.) the ion hits a molecule on the surface or below, the energy is propagated through a chain of molecules in one of the planes of closest packing and the last member of the chain is ejected.

According to this theory the sputtering yield is given by

$$S = (\bar{E}/4E_d) \left[1 + (\ln \bar{E}/E_s)^{1/2} / (\ln 2)^{1/2} \right] \sigma n^{2/3} ,$$

where \bar{E} is the average energy transferred from the ion to the target, E_s is the latent heat of sublimation, σ is the collision cross section, and n is the number of atoms per unit volume. E_d is the energy needed to displace an atom from its lattice site and for a typical tightly bound solid it is $\approx 5\text{ev}$ for the bulk and $\approx 2\text{ev}$ for the surface²³.

Experimental evidence in the low energy range is abundant for the support of this theory. On single crystal targets the ejection patterns very closely relate to the crystal orientation. The deposit "patches" resemble the patterns produced in a field ion microscope²⁴. An extensive treatment of this focussing effect both in its theoretical and experimental aspects is given by Garber and Fedorenko²⁵. This ejection pattern cannot be explained on the basis of either of the other mechanisms. Polycrystalline targets sputter according to the cosine law under normal ion incidence, but when the bombardment is oblique, ejection occurs preferentially in the forward direction. At an angle of incidence greater than 45° however the preference changes to the backward direction. When sputtering yields for different materials are plotted against atomic number a periodicity is observed and the graph shows a striking similarity to the heat of sublimation, when that is plotted in a similar manner. (Figure 9).

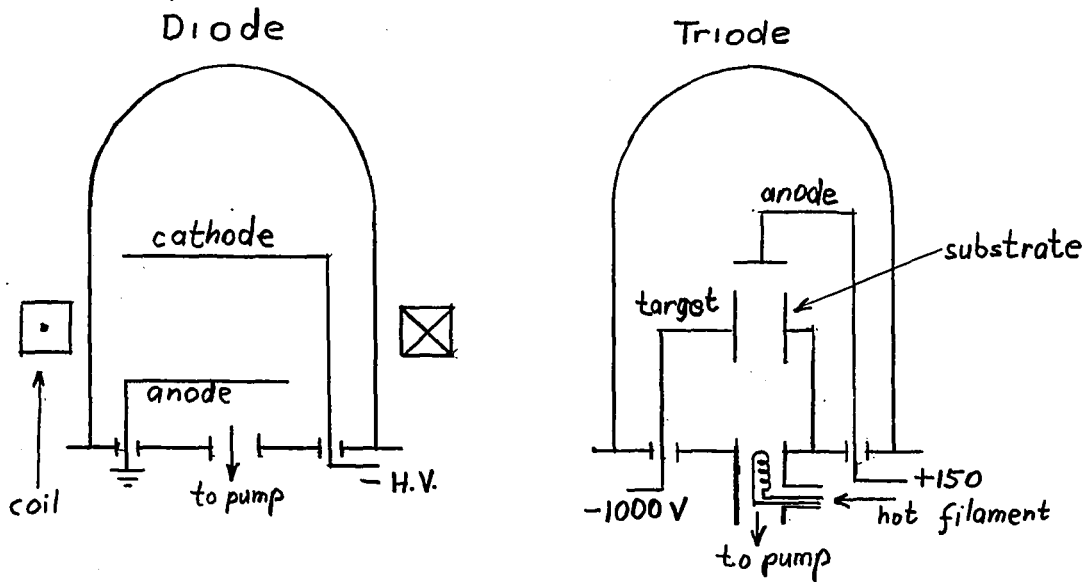


Figure 10 - Basic Sputtering Configurations.

A variation on this theory is given by Keywell²⁶ who derived a yield formula on the basis of the neutron cooling mechanism. Here an incident ion, when it approaches a target atom, creates a local disturbance which results in a loss of momentum to itself. The disturbance propagates to the surface, and if it has sufficient energy it removes an atom. The formula given (which agrees well with experimental facts) is :

$$S = (E_o/E_s) F(M_1/M_2)$$

where E_o is the energy of the incident ion, E_s is the target heat of sublimation, M_1 and M_2 are the ion and target atom masses respectively and F is a rapidly converging function with one term for each collision suffered by the ion. According to the formula heavy ions are better suited for sputtering purposes than light ones, thus the popularity of argon, which is one of the least expensive of the noble gases, but is heavy.

Sputtering yield is however not the quantity of main importance in practical work but the deposition rate. Provided that the yield is known the amount of deposited

material can be regulated by adjusting the pressure and the inter-electrode distance.

Calculations are simplest for a plane-parallel cathode-anode setup (most units utilize this system because it confines the discharge and results in uniform films) :

$$Q = K/dp ,$$

where Q is the amount of material deposited per unit area, d is the inter-electrode spacing, p is the pressure and K is the system constant, dependent on target conditions, yield, geometry, etc.²⁷ The difficulty in using this formula comes from the fact that the voltage necessary to maintain the discharge depends on pressure. But K can be kept constant within reasonably wide limits with the help of a variable intensity magnetic field, parallel with the electric field, which increases the ionization efficiency by making the electrons spiral and thus permits keeping V constant. Without this external field the voltage must be taken into account :

$$Q = K_2 V/dp .$$

This however is only an approximation, because the number of liberated electrons at the cathode surface is not a linear function of V and thus neither is Q , but the approximation is valid in the 1-5 Kev ion energy region.

4.4 Methods of Sputtering

"High pressure " sputtering is carried out in the 20-100 micron pressure range.

As mentioned above, the usual arrangement involves plane-parallel electrodes, with the anode grounded and serving as the substrate holder. If the anode were positive and the cathode grounded (or neither grounded) then the glow discharge would not be confined to the interelec-

trode space and sputtering from all metal supports and walls would result. With grounded anode there may be electron currents flowing to other elements in the chamber at ground potential but the electrons do not possess sufficient momentum for dislodging particles, and causing contamination.

By deviating from the large area parallel electrode arrangement prediction of the system behaviour becomes difficult. The ejection pattern is no longer the cosine distribution, deposits become nonuniform and the distortion of equipotential lines may result in localized glows and localized ignition of arc-discharges. Naturally this fact can be used to advantage in special cases. For instance to ignite a glow at low pressures and voltages, where the plane parallel structure would not support a discharge a sharply pointed element may be employed, that is withdrawn once the glow is struck. A coil is usually placed around the bell jar, in such a fashion that the magnetic and electric fields are parallel and coincide in space. Relatively low magnetic fields will greatly influence the current density. The author found that a coil of 3000 amp-turns on a 21 " diameter circle (≈ 40 gauss) will change the current density by 20% at 20 microns in a 50-50 argon-oxygen plasma. Close placing of the substrate and the target increases the deposition rate, but this is only possible within narrow limits, because if the anode is the substrate, then entering the dark space will extinguish the glow and if the substrate is separated from the anode then, by its own bulk, it will shield the target from bombardment.

Shielding of the back of the cathode and of the high voltage lead is achieved either by insulator coverings or by the placing of a grounded metal shield so close to these parts, that it is within the dark space and thus prevents a discharge.

To reduce absorption of the backfilling inert gas into the deposited film "bias sputtering" is frequently used. This consists of the application of a small negative potential to the substrate during coating. By maintaining the cathode at a much higher negative potential, the reduction in yield is negligible. This small scale back-sputtering from the substrate is effective because the trapped gas molecules are removed at a much higher rate than the film material and the gas is freed not only by momentum exchange but also by thermal spiking²⁸. The disadvantage of bias sputtering is that it disturbs the crystallization process of the film, and the resulting structure is unpredictable.

"Low pressure sputtering" is achieved with the help of a hot cathode and relies on thermally emitted electrons to support the plasma (see Figure 10). An anode plate with a small positive potential (1-200v) is placed opposite the heated filament. The large amount of thermal electrons permits ionization at pressures below one micron. The target, which is now separated from the cathode is placed facing the substrate (also separate from the anode) on either side of the discharge column. When a negative potential is applied to the target the electrons in the plasma are repulsed and form a visible Langmuir sheath, while the positive ions accelerate in this electron-free region and bombard the target. There are several advantages to this system. Lower pressures result in less absorbed gas and less porous films, independent control of pressures, voltages and currents is possible, target-to-substrate distance may be adjusted as desired (no dark space), initial clean-up of target and substrate is possible via ion scrubbing without the need for a shutter because plasma can be established without sputtering setting in. The disadvantages are mechanical complexity, the need for an additional power supply and the periodic deterioration of the filament.

"Radio - frequency sputtering" is necessary for the deposition of dielectrics. In

the above mentioned methods an insulating target quickly accumulates a positive surface charge and blocks the ion current. If, however, the target bias is periodically removed or reversed, then this surface charge can be neutralized. On the first half cycle of the applied bias (say it is positive) an electron current will flow toward the target, while on the second half cycle an ion current will be drawn. Since the electron mobility is several times larger than the ion mobility, if polarity is reversed sufficiently fast, the electron current will exceed the ion current. This results in a continuously increasing net negative surface charge until an equilibrium value is reached, about which the RF bias oscillates. At this point ion current will flow for more than half of the total cycle to compensate for the higher intensity of the electron current. The potential of the dielectric surface, for the time when it is negative, will decrease in absolute value at a rate given by :

$$(dV/dt) = i_1/C$$

where i_1 is the ion current and C is the target capacitance, typically of the order of 20 pf/cm^2 . For an ion current of, say 2mA/cm^2 , this results in $(dV/dt) = 10^8$ volts per second. Now, if one cannot tolerate more than a decrease of 100 volts, then the frequency must be in the megacycle range. It has been found by Anderson²⁹, that the RF bias will cause a spread in ion energies about the equilibrium value and, unless the frequency is above 10Mhz, this spread is detrimental to the sputtering rates. The negative self-bias reached by the insulator can be created on a conducting target, too, simply by putting a blocking capacitor in series with the probe.

If the backfilling gas is not inert, a chemical reaction can be made to occur between the sputtered particles and the gas. "Reactive sputtering" is a process utilizing this effect. Nitrides, hydrides and oxides are the more common materials prepared this way.

The process is applicable to either of the above described methods. Reactively sputtered oxide films are invariably adhesive to glass and have a very fine grain structure. Their optical and physical properties depend on the partial pressure of oxygen. No detailed studies are available on the mechanism of reactive sputtering. The only known facts are, that

- (a) the inclusion of an electronegative gas (O_2) changes the nature of the plasma and causes a considerable portion of the sputtered atoms to acquire a charge,
- (b) the higher the percentage of O_2 the smaller the crystal size of the deposit,
- (c) for most materials (Zn among them) the resistivity of the film has a strong dependence on oxygen content (exponential within limits).

It is not known where the oxidation takes place, but if the partial pressure of oxygen is larger than a few microns, the target surface will usually be covered with a layer of oxide. Low pressure sputtering is not well suited to reactive sputtering because the chemical reaction will enhance deterioration of the hot filament.

CHAPTER V

EXPERIMENTAL APPARATUS AND PROCEDURES

5.1 Sputtering Unit

The design intent behind the sputtering apparatus was to create a flexible unit that would permit the study of the influence of the various sputtering parameters on the properties of the deposits.

The basic vacuum system utilized was an NRC No. 3116 Coater with an 18 " bell jar and a 6 " oil diffusion pump. Without any fixturing in the bell jar a vacuum of 10^{-6} torr could be reached within 30 minutes and 10^{-7} torr in several hours. The exact time to reach a particular pressure depends on how long the system was exposed to the atmosphere prior to pumpdown and on the ambient conditions. To permit easy access to the diffusion pump for cleaning purposes the apparatus was made portable by building it onto a feedthrough ring rather than onto the baseplate.

5.2 Electrical Connections

The high voltage lead was a solid S-shaped 3/8 " brass rod insulated from the feedthrough ring by a vacuum-tight ceramic tube. (Figure 11 is a photograph of the apparatus.) The upper end of the high voltage rod is above the center of the base plate and it is attached to a 2.25 " diameter brass disc. This disc serves as the actual voltage supply to the various cathode materials and as a heat sink. During sputtering up to 500 watts of power is delivered to the cathode and, for low melting point materials like zinc, it is necessary to provide some means of cooling. For this reason the brass plate and the end

portion of the high voltage lead were enclosed in a delrin water jacket. The water is brought through the feedthrough ring in tygon tubes and is in direct contact with the high tension electrode. A ten foot long column of 3/8 " diameter tapwater has sufficient resistance to make any power loss negligible. To prevent sputtering from anywhere but the cathode the high voltage lead is enclosed in a tight fitting tygon tube between the water jacket and the ceramic insulator.

For good adhesion between the delay line, the metal film electrodes, and the zinc oxide film it is advantageous to be able to deposit all films in a sequence without breaking vacuum and without large changes in the temperature of the substrate. A rotary cathode holder makes the sequential sputtering of three materials possible. This holder was cut out of a teflon plate, had a circular shape, and three holes of 2.25 " diameter were cut into it. Each hole carried a press-fitted vycor tube, the upper end of which was slightly flared to form a seat for the source material. The teflon plate (1/2 " thick, 7 " diameter) was supported by a spring-loaded, ratcheted brass rod, which could be rotated by a mechanical linkage from outside the bell jar. As the cathode rotated into position under the high tension plate the two were pressed against each other by the spring. By applying torque against the linkage, the plate was lowered first and then the next cathode was brought into contact with the supply. This spring loaded arrangement was necessary to maintain good thermal contact between the source and the cooling head.

A 2 1/4 " x 1/2 " x 1/8 " aluminum ring served as the anode. It was insulated from its support by an asbestos insert which was used, inspite of the tendency to outgas heavily in vacuum, to avoid having to cool the anode. Electrical insulation of the anode support and the floating of all fixtures helped restrict the discharge between the electrodes.

The substrate holder was an aluminum cylinder and the crystals were clamped inside it by half-moon shaped, spring-loaded metal blocks to ensure good thermal contact. Heat was supplied to the crystals by a resistance heater, controlled from an external variac, placed under the substrate holder. Care had to be taken to insulate the heater supply leads thoroughly inside the vacuum to prevent the creation of a discharge between these leads and the cathode. The heater-holder assembly sat inside the anode ring and could be floated or grounded to the anode as desired. A continuous adjustment of the inter-electrode distance and of the substrate position (vertically) could be effected from the outside.

A shutter placed between the cathode and the substrate served as mask for controlled area deposition. It rode vertically with the substrate to ensure constant (preset) separation between the two, which is necessary for masking. Several metal masks of varying sizes were carried by the shutter arm and could be rotated above the substrate without breaking vacuum. Accurate positioning was achieved with a click-stop arrangement.

5.3 Operating Procedures

Sputtering was carried out under a steady flow-through of gas and constant internal pressure was ensured by balancing the gas leak valve against the diffusion pump valve. When maintaining a dynamic pressure above 20 microns the backstreaming of oil became noticeable by forming a thin film of oil on all the cooled parts, but this unwanted effect was greatly reduced by placing a variable-opening, water-cooled baffle over the pump throat.

X-cut and Z-cut quartz and Z-cut sapphire crystals of $1/4" \times 1/4" \times 1/2"$ size were used as substrates. After several trials Z-cut quartz was abandoned because the

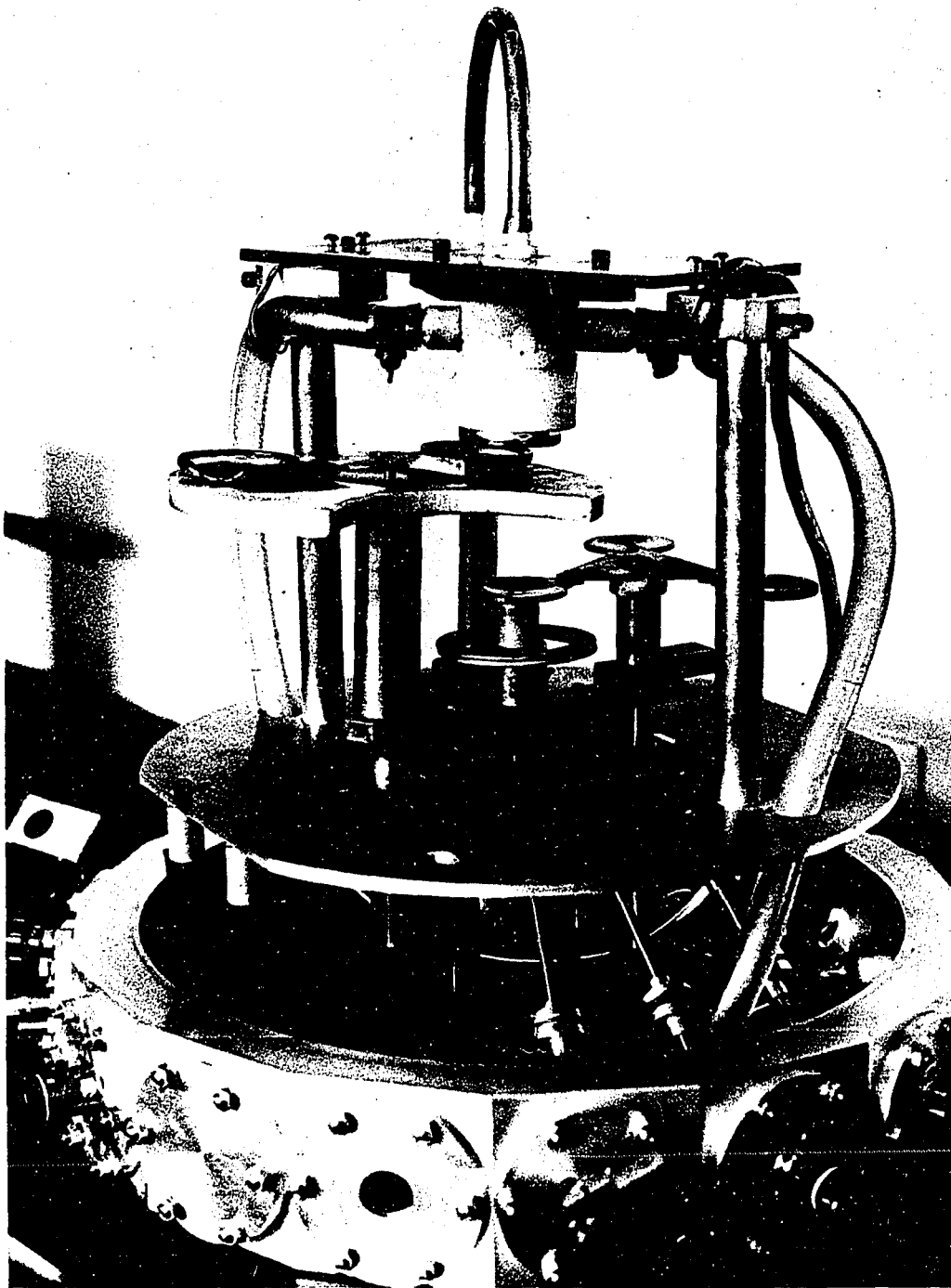


Figure 11 - The Sputtering Unit.

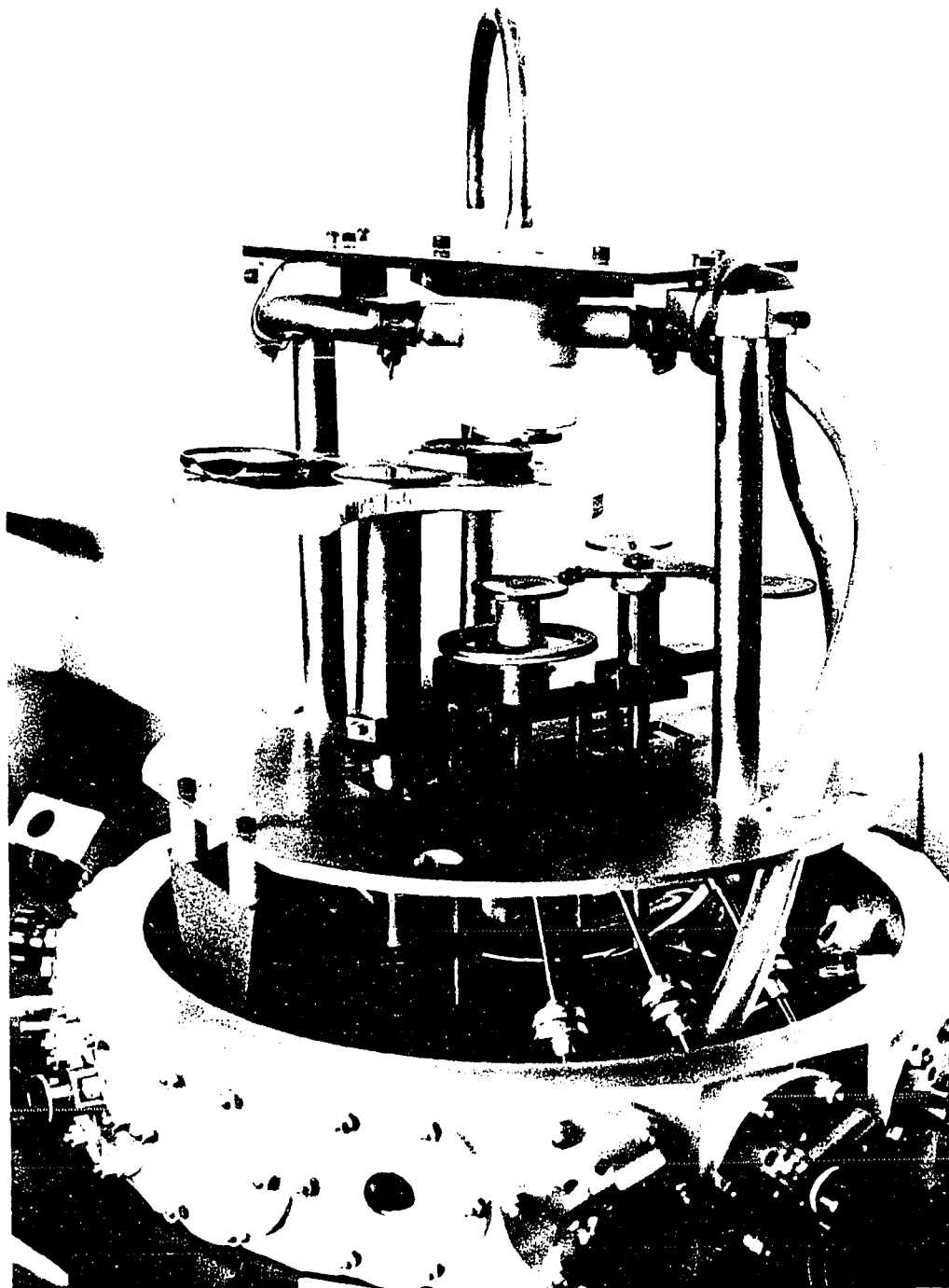


Figure 11 - The Sputtering Unit.

difference in the thermal expansion coefficients of ZnO and of quartz in this direction is too large and a temperature change of 30°C or greater shattered the deposits. Gold was chosen as the bottom electrode of the transducers because of its good electrical and chemical properties. Since gold does not adhere well to quartz or sapphire, a good oxide forming metal must be deposited between it and the crystal, and, in these experiments, nickel, nichrome or chromium were used. An iron-constantan thermocouple embedded in the substrate holder and touching the side of the crystals about 1/8" below the surface was employed for measurement of substrate temperatures.

5.4 Sputtering Difficulties

Several difficulties were experienced with the above unit. The teflon, delrin and tygon insulation of the high voltage leads (used in place of ground-shielding for mechanical simplicity) broke down repeatedly over 3000 volts, although it could be used up to 4000 volts under certain circumstances. The teflon plate holding the cathodes overheated near the plasma and became a source of continuous outgassing and contamination. After a few minutes of sputtering the vycor seats were coated with a film of the source material and thus having acquired a surface conductivity close to that of the source, they acted as secondary cathodes. Since the seats were not in contact with the cooling head, hot spots developed under ion bombardment and eventually both the metal film and the vycor boiled off, causing severe arcing.

Deposition through the rotating masks was found to be impractical because, in order to permit smooth rotation, a minimum distance of 0.020" had to be maintained between the substrate and the mask and at this distance the diffraction off the mask edge was enough

to create fuzzy, ring-like patterns. A thin foil mask placed directly on top of the substrate gave sharp deposit boundaries but the film acquired a lens shape, considerably thicker in the center than around the edges.

These difficulties could be handled at the cost of some inconvenience (such as abandoning the masks in favour of post-deposition chemical etching, etc.), but the presence of the large amount of fixturing inside the bell jar led to slow pump-down and pressures lower than 5×10^{-6} torr could not be reached within practical time limits.

5.5 Adhesion of Gold to Substrate

Even with a nickel or chromium under-layer the adhesion of gold to substrate was very poor when sputtered in an argon plasma, probably because the outgassing of the fixtures introduced enough oxygen into the chamber to oxidize the nickel. A pre-sputtering in hydrogen for ten minutes at high pressures (100 - 200 microns) and normal sputtering following it in 10% hydrogen-90% argon solved this problem and provided films of excellent adhesion. The gases could either be mixed inside the bell jar by introducing them through separately controlled needle valves, or be premixed. The argon-oxygen mixtures used in reactive sputtering of zinc oxide were obtained commercially, premixed in bottles.

5.6 Substrate Cleaning

The films were not overly sensitive to differences in the cleaning procedure from the point of view of adhesion. (This was only true for sputtered and not for evaporated films, which were also used as electrodes in some experiments.) The general cleaning of substrate crystals consisted of the following steps :

- (a) boiling in a mixture of trichloroethylene and isopropyl alcohol for two minutes,
- (b) immersion in aqua regia or hot hydrochloric acid for one minute,
- (c) short rinse in distilled water to remove the acid,
- (d) several minutes treatment in a vapour degreaser (Minivap) utilizing isopropyl alcohol as solvent.

Several films of acceptable adhesion were prepared by omitting all but the first step in the cleaning procedure, but this did degrade reproducibility. The acid treatment is included mainly because the substrates are used repeatedly and this removes the previous deposits. In the case of new crystals it is useful because it removes dust and metallic particles. The acids effect the surface polish of the crystals however, and therefore the immersion is to be kept at a minimum.

5.7 Thickness Measurements

It is readily seen from the theoretical treatment of transducer performance, that the film thickness must be accurately known if the behaviour of the device is to be predicted. There are several widely used techniques of thickness measurement in the micron range belonging to two main groups: those that measure film thickness while deposition is in progress and those that permit measurement only after the deposition has been concluded. For industrial purposes the first group is clearly preferable, but in the laboratory post deposition measurements can be totally adequate, especially for sputtering where the increase in film thickness is linearly dependent on time.

One of the most widely used in-process monitors is the crystal oscillator. It operates on the principle, that when a (quartz) crystal is excited to thickness shear oscillations, any change in mass will cause a proportional shift in frequency. The crystal is placed in the path of the sputtered particles and from the change in its frequency of oscillations the mass of the deposit is determined. Some of the difficulties with this instrument are : bulkiness, sensitivity to temperature variations and interference of the sputtering field with the crystal's own electric signals. The microbalance is another, and from the point of view of sputtering, probably more useful, instrument in this group. One arm of the balance holds a small plate in the deposition beam, while the other arm is attached to a spring or electromagnet, giving an indication of the weight of the deposit from which the thickness can be calculated. Both of these methods assume that the density of the film is equal to the source-density, which is not necessarily true. There are a number of other, usually more complicated, devices that rely on changes in resistance or in optical properties to measure thickness, but since such changes are pronounced only for certain materials, these methods have a limited applicability.

In this experiment an instrument belonging to the second group, the Taylor-Hobson Mitronic Differential Comparator, was used. It consists of two metal balls, that are dragged across the substrate at the ends of spring loaded levers the deflection of which is electrically sensed. Distance between the balls is kept as small as possible without touching. For accurate measurement it is necessary that the deposits have an abrupt edge. One of the balls is rested on top of the film, the other is on the substrate and this latter is the reference with respect to which the elevation of the other is measured. By moving the two sensors in unison any unevenness in the substrate is eliminated from the results. The device gives thickness values with a 10% uncertainty in the $1/2 - 10$ micron range. Most

of the uncertainty came not from the instrument but from the substrate support. The abrupt edges were prepared by etching the zinc oxide through a wax mask with hydrochloric acid, after which the wax was washed off in trichloroethylene. The deposits were generally hard enough not to be damaged by the sensors, but bits of the exposed gold were often dragged onto the ZnO and smeared across it.

Films less than 1/2 micron thick were measured with a Fizeau plate-type optical interferometer utilizing green light of 5350 Å wavelength. Optical post-deposition techniques are superior in accuracy to mechanical ones, but the zinc oxide, when deposited at high rates, was not sufficiently reflecting for the method to be useful without metallizing the top surface.

Optical measurements of the same order of accuracy as the mechanical ones were carried out by focussing a microscope on the top and bottom of the films and reading the difference on the calibrated focussing button. Accuracy with this setup could be improved by employing a lens of higher magnification and shallower depth of field.

5.8 Determination of Insertion Loss

There are two direct methods available for the determination of the insertion loss of a piezoelectric transducer.

(a) In the "transmission method" both ends of a suitable delay line are equipped with a transducer, one of which serves as a generator and the other as a receiver of acoustic waves. The power loss from the input to the output electrical signal is the insertion loss of the entire device and from this the efficiency of a single transducer can be calculated. The inherent difficulty of this method is that two transducers have to be made

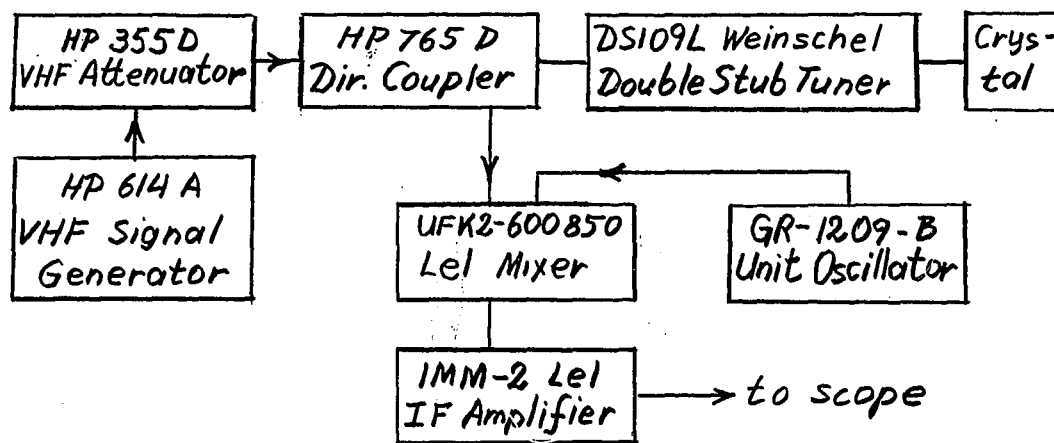


Figure 12 - Block Diagram of PEM Setup.

and only the average of their efficiencies can be obtained. The relative position of the receiver with respect to the generated acoustic beam is critical and thus preparation is difficult. The advantage is that continuous wave operation is possible and that electrical generating and detecting equipments are isolated from each other by the delay line.

(b) With the "pulse echo" technique³⁴ the same transducer is used for generation and detection of acoustic signals. The transducer is deposited on a delay rod and is excited by an R. F. electric pulse of sufficiently short duration to be well separated in time from its own echo being reflected by the other (free) end of the rod. Separation of the signal from the echo and isolation of the generator from the receiver are the main problems, since both of these are connected across the same pair of electrical terminals. A directional coupler can give 20-30 db separation between the two signals and other devices, such as a hybrid are capable of doubling this figure. The generator in this experiment was matched to the transducer at all frequencies with a double stub tuner. A block diagram of the actual setup is shown in Figure 12.

CHAPTER VI

EXPERIMENTAL RESULTS

6.1 The Effect of Sputtering on Different Cathodes

Zinc oxide films were prepared from zinc metal and from hot pressed powder zinc oxide sources made into 2 1/4" diameter, 1/2" thick plates. The area from which actual sputtering took place was controlled by shields placed in front of the cathode to produce certain combinations of voltage-current-temperature operating values. Without shields a high applied voltage combined with high pressure resulted in high power dissipation and, since the substrate had no cooling system, in elevated substrate temperature.

The metallic zinc sources were made from sheet metal and rolled rods. After several hours of use the sheet source developed an irregular, large size (4-6 mm average diameter) grain pattern and the rod source showed an etch pattern radially outward from the center. A freshly cleaned cathode surface remained shiny and metallic when used in 2% O₂ - 98% Ar atmosphere, but developed a thick, clearly visible coating of white, semi transparent oxide when the oxygen content of the gas was increased to 50%. In all cases, however, with a constant applied voltage, the discharge current decreased 10-25% from its initial value within 5-10 minutes. This could either be the result of oxidation of the cathode or, more probably, of a release of gases adsorbed on the electrode surface, causing a local increase of pressure and thus of ionization efficiency. The same phenomenon was observed with the pressed-powder cathode, but since it was more porous than the metal the effect here is more probably due to outgassing.

Freshly cleaned zinc oxide cathodes had a light yellow colour which remained unchanged when sputtered at low rates and in a highly oxygenated atmosphere, but turned brownish with increased sputtering rates and greyish when oxygen content was reduced to 2%, indicating a zinc enriched surface layer. There may be a two fold reason for this : either the zinc oxide was not sputtered as a compound, or the surface overheated locally. Thermal contact between the cathode and the cooling head was generally very good, but a 1/2" layer of compressed oxide powder can act as a high enough thermal insulation to cause localized heating of the surface. On opening the bell jar, the cathode temperature was never over 100° C, but since the process of opening took several minutes the incoming air may have cooled the surface considerably.

6.2 Establishment of the System Constant

Figure 13 shows the rate of deposition of zinc oxide from a sheet metal zinc source as a function of the applied cathode voltage in a 50% O₂ - 50% Ar atmosphere. The pressure was kept at 35 microns and the temperature was constant at 220° C in this series of experiments. It was generally impossible to regulate the temperature to better than ± 10° C and the pressure to better than ± 3 microns in the initial hour of deposition and, since the individual experiments rarely exceeded 2-3 hours, the results include at least half of these uncertainties, plus the errors from the thickness measurements. These remarks apply to all of the results and, within experimental error, the graph shows a linear dependence of rate on voltage.

The relationships between cathode to substrate distance, rate of deposition and

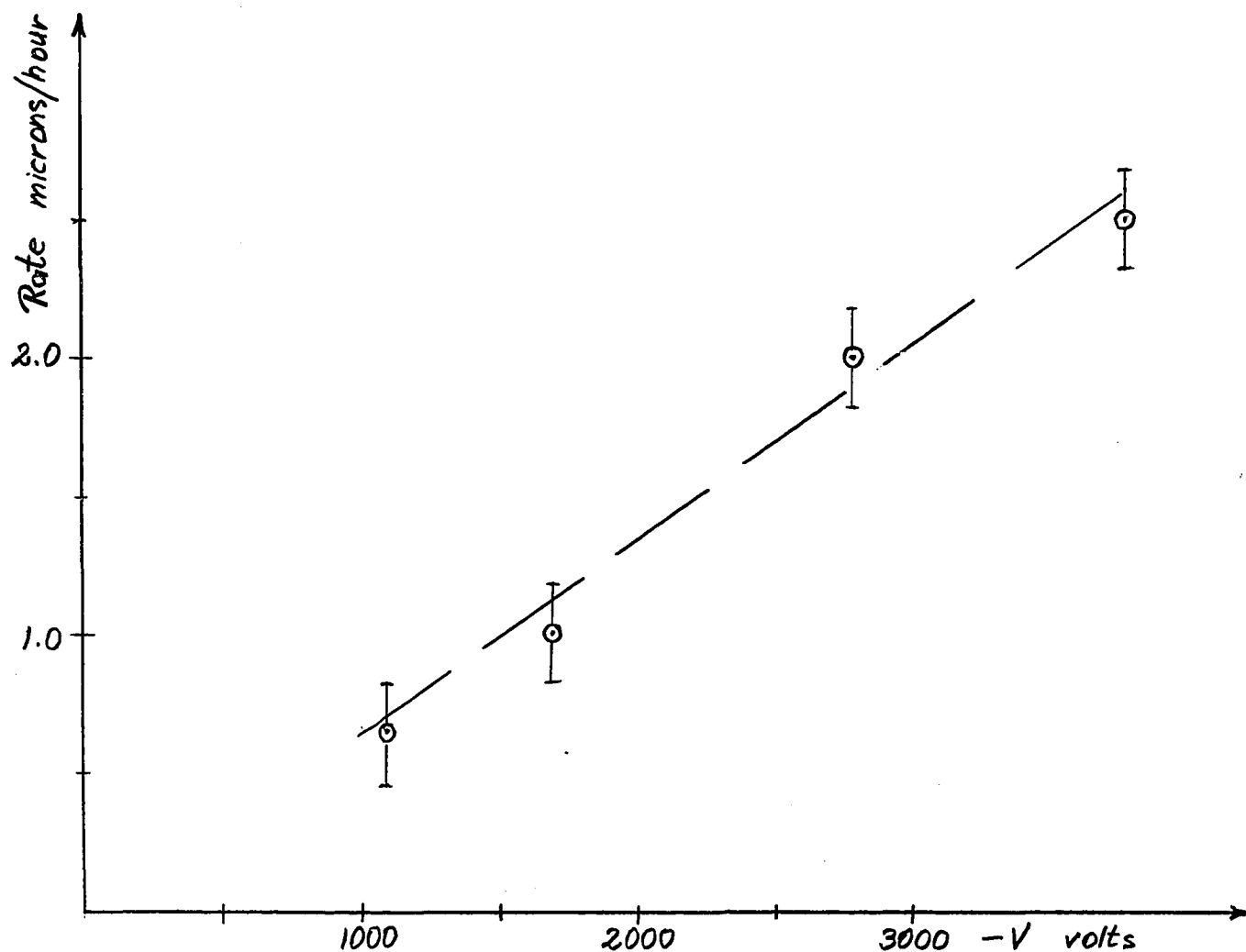


Figure 13 - Rate of Deposition vs. Cathode Voltage.

sputtering pressure are given in a combined form on Figure 14. This is a convenient presentation, since the pressure and the minimum distance necessary for the maintenance of the discharge are dependent on each other. At low pressures the dark space expands and if the substrate is inside the dark space it shields the cathode above it from bombardment, and this leads to erroneous results. Therefore the substrate was kept in the positive column.

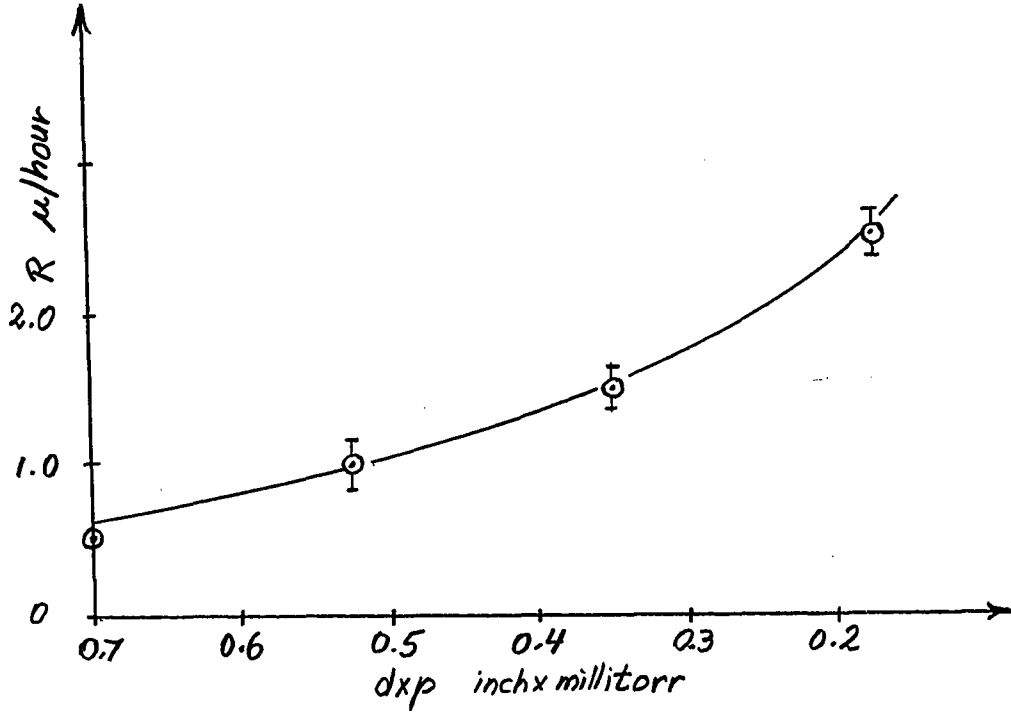


Figure 14 - Rate of Deposition as a Function of Cathode to Substrate Distance and Pressure.

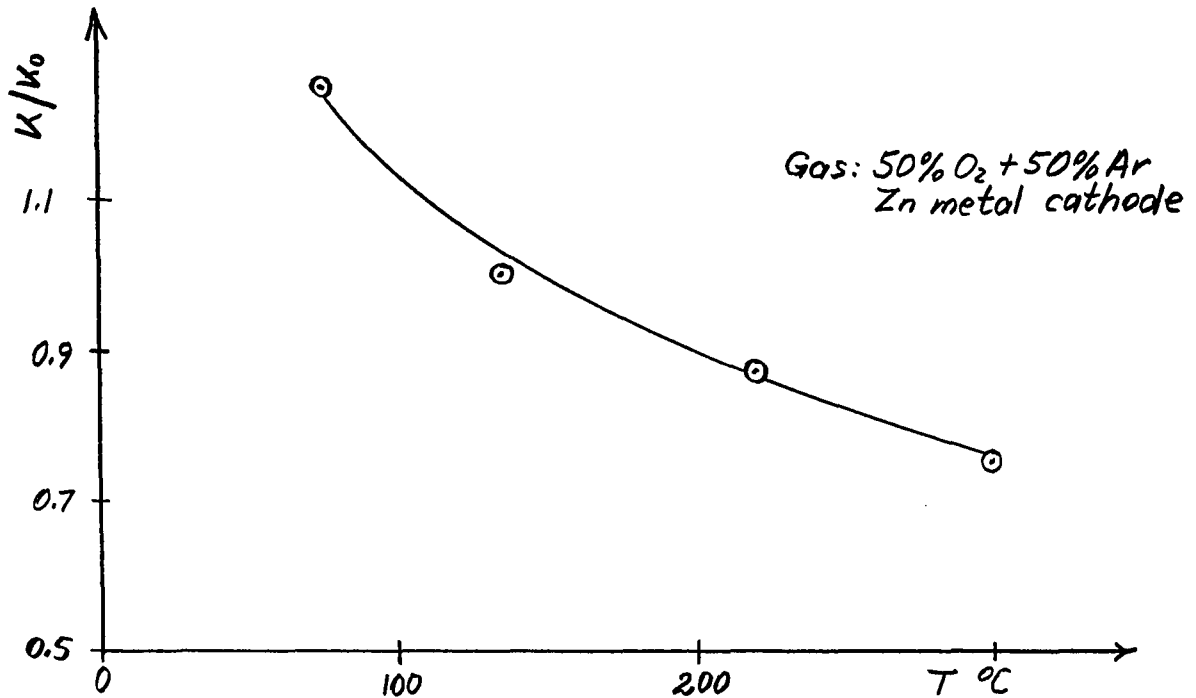


Figure 15 - Variation of System Constant with Substrate Temperature.

The deposition rate was found to be inversely proportional to the product of pressure and distance.

Figures 14 and 15 combined show an overall behaviour of the form :

$$R = K_s \cdot V/d \cdot p,$$

where R is the rate of deposition and K_s is the system constant, while d and p are the distance and pressure respectively. This pattern is in agreement with that established by other workers (see Chapter IV).

6.3 Effect of Temperature on the System Constant

The system constant exhibited a marked dependence on the temperature of the substrate but due to the narrow temperature capability of the heating element this dependence could only be examined from 75 to 300°C. In this interval the curve of Figure 15 is represented by the exponential equation

$$(K_s/K_0) = 6.1 (T^{-0.366}), K_0 = 27,$$

where the units of temperature are degrees centigrade and K_s is in (micron x inch x millitorr)/ (kilovolt x hour). The units of K_s are the same in all of the following graphs. Lack of published information for sputtered zinc oxide relating to this curve prevents any direct comparisons, but results of a similar nature were published by Maissel³⁵ for sputtered germanium.

When a particle arrives at the substrate surface it may transfer most of its energy to the surface and remain stationary at its point of impact or retain sufficient energy to

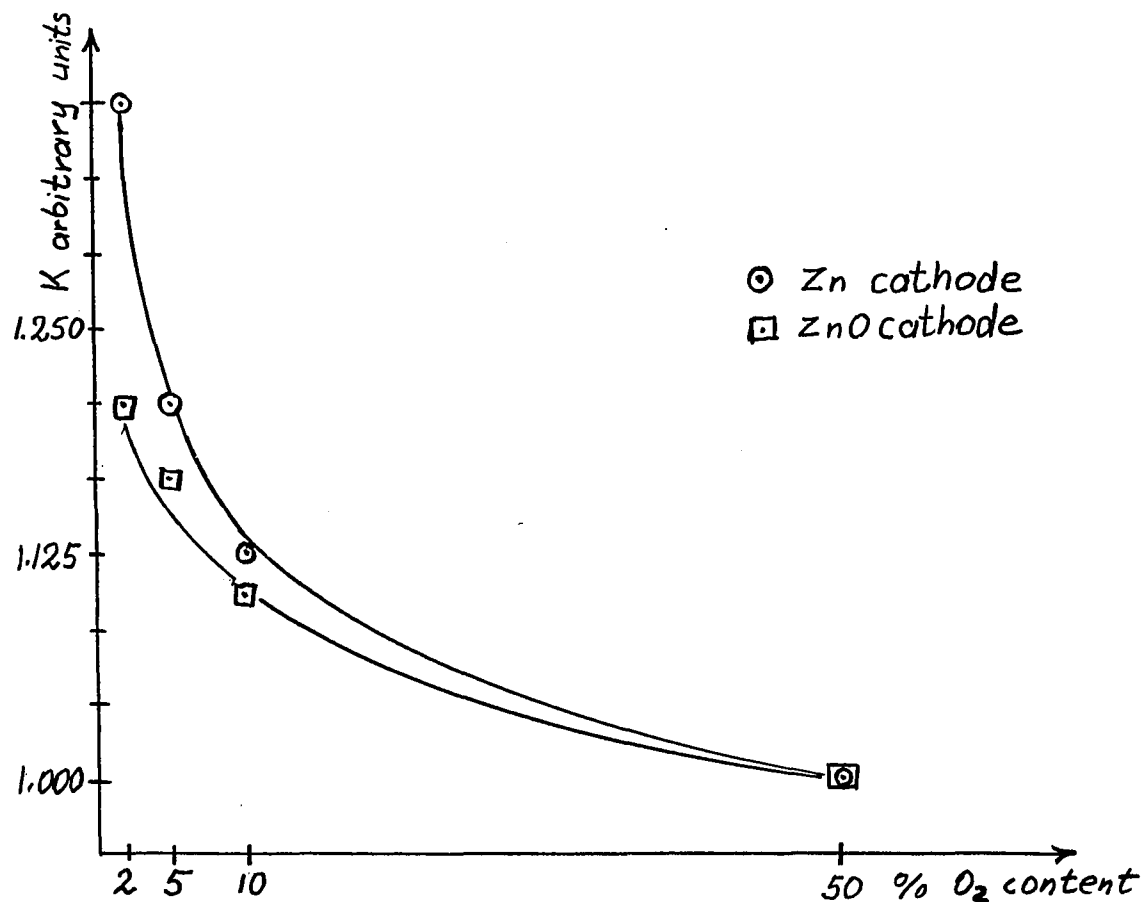


Figure 16 - Variation of System Constant with Oxygen Content of Sputtering Gas.

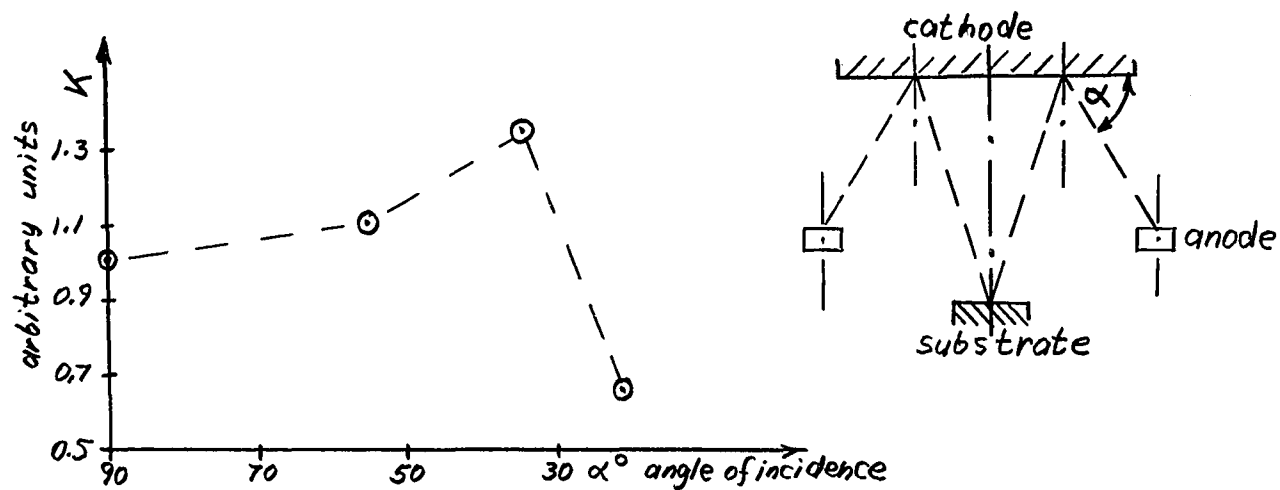


Figure 17 - Effect of the Angle of Bombardment.

move about over the surface without actually leaving it, or it may rebound from the substrate. Suppose that most of the arriving particles belong to the second group. If their energy distribution is normal (which is to be expected, since in high pressure sputtering the particle suffers a large number of collisions before reaching the substrate) then an exponential dependence on temperature is readily explained. To be able to give a detailed picture of the process, the experiment would have to be carried out over a much wider temperature range. Re-evaporation is not likely to come into play because of the high melting point of zinc oxide.

6.4 Effect of Oxygen on System Constant

The rate of deposition is influenced by the gas mixture in the chamber and while an increase in oxygen content causes a greater fall-off of rate for metallic cathodes it is also appreciable for an oxide source. This leads to the conclusion that while most of the reduction in K_s is due to an increase in resistivity of the more thoroughly oxidized cathode surface, it is partially due to the change in nature of the ion beam. Oxygen is an electro-negative gas and when the plasma is mainly in argon most of the oxygen will be present in the form of negative ions around the anode. When the O_2 content is high, however, a considerable portion of the ions reaching the cathode are oxygen ions. The atomic weight of oxygen is less than that of argon and thus the yield per incident ion is smaller. The difference in curves for Zn and ZnO cathodes (figure 16) is largest at the low oxygen content end where oxidation of the zinc metal surface is likely to be most important.

6.5 Angle of Ion Incidence

The mechanical as well as electrical separation of the anode and the substrate holder permitted some checking of the effect of the angle of bombardment on the deposition rates. The setup was not ideal for this purpose because of the ring shape and large size of the anode, and comparison with other published data cannot be made for this reason. Figure 17 contains the results of the measurements and the insert shows how the angle was determined. The variation in K_s is noticeable with highest deposition rates occurring between 30 and 40 degrees of ion beam incidence.

6.6 Resistivity of the Deposited Films

The electrical resistivity of the zinc oxide films was mainly dependent on the rate of deposition and the oxygen content of the sputtering gas. The effect of other parameters (such as temperature) could not be separated out due to the limited accuracy of the measurements. Experiments were performed with both the Zn and ZnO cathodes and the results are presented in Figure 18. For higher than 2% O_2 content the curves for both sources are so close together that the difference can be accounted for by experimental errors. For less than 5% oxygen in the sputtering gas the curves are plotted separately for both sources. The resistivity vs. growth rate curves have an exponential form for the ZnO cathode, the exponent being smaller for higher oxygen content. For a metallic cathode and low oxygen content, the deterioration of resistivity is more pronounced, decreasing faster at the high growth rate end of the scale. At present there is no explanation available for this behaviour, since even with 98% argon in the gas there is enough oxygen present to oxidize

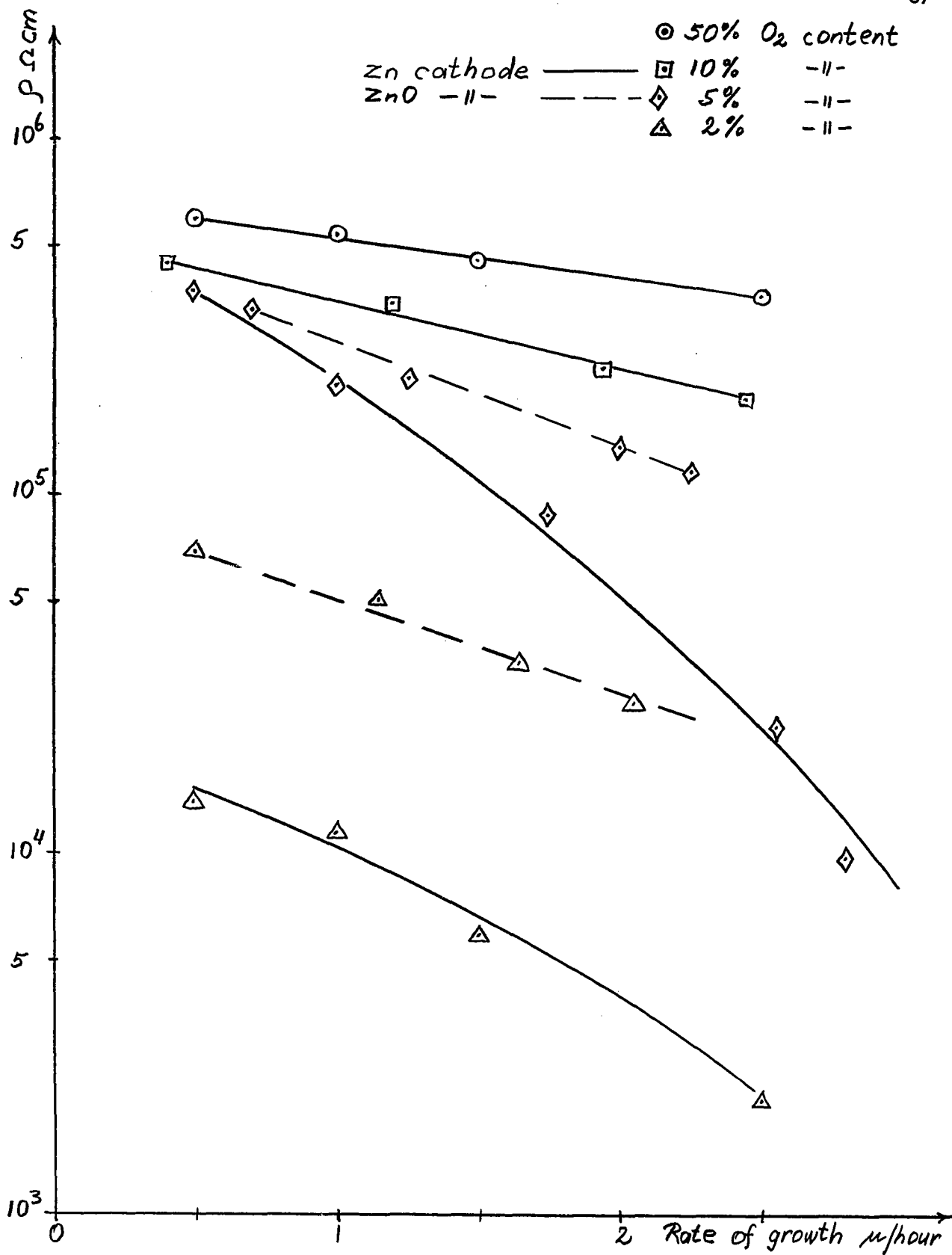


Figure 18 - Relationship between the Resistivity of ZnO Films and Growth Rate.

all arriving Zn molecules at all of the tested growth rates.

The appearance of the films was related to the resistivity and growth conditions in the following manner :

<u>Film</u>		<u>Appearance</u>
high res., high rate	-----	milky, semi-transparent, matt
low res., high rate	-----	more transparent, blue-grey matt
high res., low rate	-----	milky, matt,
low res., low rate	-----	glassy, transparent, slightly blue

The most glassy and clear specimens were produced when the low growth rate was determined by high pressure rather than one of the other variables. When the top of a high resistivity film was gold plated in a 10% H₂-90% Ar discharge (instead of in pure argon) the zinc oxide turned blue-grey and its resistivity dropped by 3-4 orders of magnitude.

Gold-zinc oxide contacts exhibited good ohmic behaviour, except at very low voltages. As an example, one such film had a resistance of 4×10^5 ohms at an applied voltage of 0.05 volts, 9×10^4 ohms at 0.30v, 8.5×10^4 ohms at 0.40v and remained steady at this value up to 20 volts.

6.7 Crystal Structure of the Deposits.

The films, even though of high resistivity, were not active piezoelectrically with the exception of one specimen. This active film was in no way different visually

from the general low deposition rate, high resistivity group and it had a rather poor adhesion to the substrate. It peeled off before accurate measurements could be performed, but five echos were observed on the pulse echo modulation setup at 800 Mc's, where it had the maximum conversion efficiency. The thickness of this film was estimated from deposition parameters to be 4 microns. The film could not be reproduced.

X-ray reflection and reflection electron diffraction (RED) techniques were used to ascertain the cause of the general lack of piezoelectric characteristics. The x-ray photos had poor resolution because the crystal size of the deposits was 250 Å or less. However, they did indicate the same structure as the RED pictures. These latter were taken at the Division of Applied Chemistry of the National Research Council on a GE diffraction apparatus using an accelerating voltage of 50 Kv and a camera length of 50 cm. The films were etched in HCl to remove any surface contaminations and diffraction patterns at different depths and at several positions in the bulk were taken. The crystal structure was uniform throughout each sample. Some preferred orientation was in evidence but it was not strong. The (110) plane of ZnO was approximately parallel to the surface with an angular spread of $\pm 25^\circ$. This is illustrated by the strong arcing of the (110) semi-ring about the normal shadow edge of the photograph in Figure 20. The (002) reflection is barely visible between the stronger (100) and (101) lines. This orientational relationship with respect to the substrate is illustrated in Figure 22. The specimen from which this photograph was taken was prepared in a 50% O₂ - 50% Ar mixture at a pressure of 35 millitorrs with an applied voltage of 2Kv and a temperature of 230° C. The entire surface of a zinc sheet cathode was utilized. The angle of bombardment and the angle of deposition were both 90 degrees, which corresponds to a large area plane parallel electrode arrangement. Figure 19 is the reflection pattern of a specimen produced under identical

Figure 19 - RED Picture of ZnO Film
Deposited from Small Area Cathode.



Figure 20 - RED Picture of ZnO Film
Deposited from Large Area Cathode.

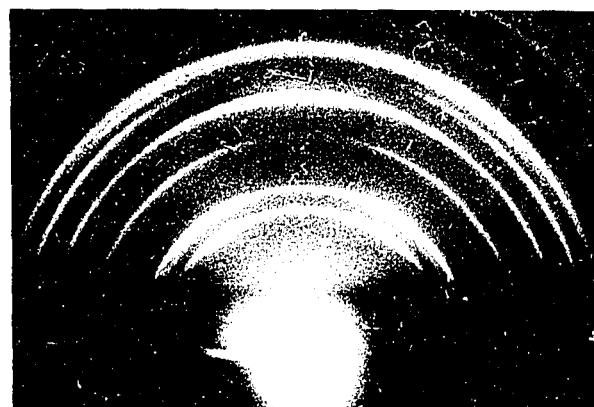


Figure 21 - RED Pattern of Sputtered
Gold Deposit.



conditions, except the cathode diameter was reduced from 2" to 1". The result is a reduction in the angular spread of the crystallites about the (110) plane to $\pm 15\%$, which can be seen from the more pronounced orientation pattern on the photograph.

Figure 22²¹ is the RED pattern obtained from a sputtered gold deposit, after the ZnO film on top of it was removed by etching. The gold exhibited a mixed fibre orientation with both the (111) and (100) planes normal to the sapphire substrate to within 10%. The microcrystallite size was estimated from line broadening as $250 \pm 50 \text{ \AA}$. Several samples were prepared on evaporated, rather than sputtered, gold layers. This type of gold was almost completely randomly oriented.

ZnO films formed in a 50% O_2 - 50% Ar mixture on evaporated gold at 40 millitorr pressure and 2-3 Kv applied voltage, but with substrate temperatures varying between 100° C and 300° C , have shown identical patterns to Figure 20. When deposited directly on polished sapphire substrates under similar conditions as above, the films had similar orientation, but smaller crystallite size. For a substrate inclined at 45° to the particle beam there was hardly any evidence of change in zinc oxide grown over gold, but on sapphire the (100) plane became tilted at $45^\circ + 40^\circ$ to the substrate. In all of these experiments, unless otherwise stated, the cathode diameter was 2".

A ZnO layer prepared on evaporated gold with 5% oxygen in the atmosphere at 25 millitorr pressure and 2.3 Kv with the substrate kept at 110° C was the only specimen to show a strong trace from the (002) plane, but with a 40° variation in inclination.

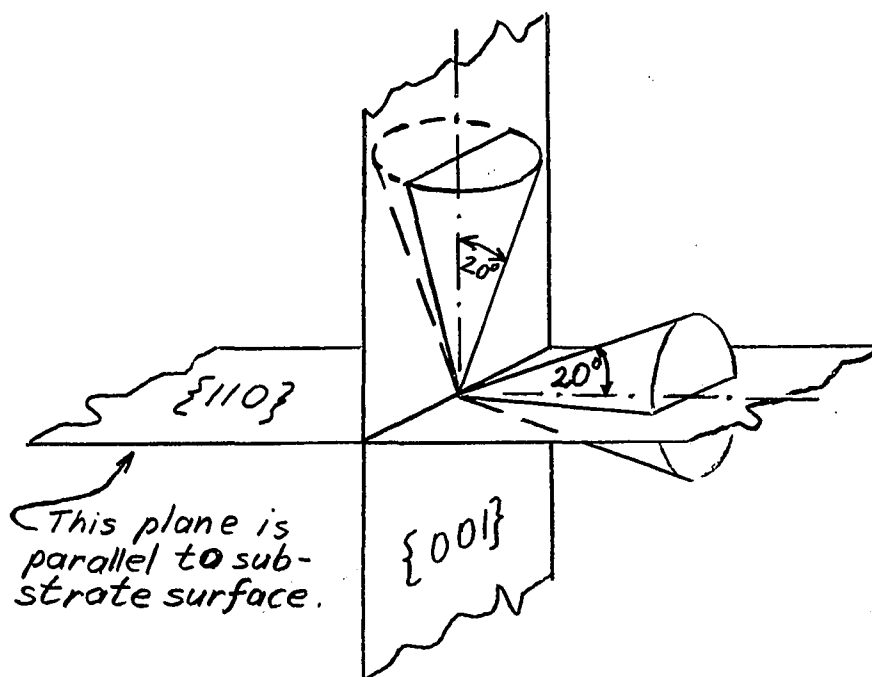


Figure 22 - Crystal Orientation of ZnO Films.

6.8 Contaminants

Films prepared from a compressed powder ZnO cathode and deposited onto microscope slides under high growth rate, low oxygen content conditions were examined by the Northern Electric Laboratories for optical emission spectra and x-ray fluorescence. The deposits were etched off the glass with cold hydrochloric acid for the optical emission test, then drop by drop dried on hot carbon electrodes. A reference sample of high purity zinc oxide powder of identical weight was taken through the same process. Both specimens were arced on an ARL 2 meter spectrograph and compared. According to this measurement the deposits contained 1-2% excess zinc, more than 1% silicon, approximately 1% Fe and Mg each and traces of B, As, Mn, Sn, Ge, Al, Cu, Ag, Ni, Ca and Pb. The x-ray fluorescence pictures also indicated 3-4% impurities other than zinc.

6.9 Discussion

The reason behind the poor orientation of the samples is not known at present. No single process variable seems to effect the growth pattern sufficiently and it is probably a combination of several factors that may eventually lead to the desired result. One can, however, point to the changes in apparatus that seem necessary to permit further insight. The present sputtering setup is not nearly clean enough to eliminate the possibility of the growth pattern being influenced by impurities in the atmosphere. The large amount of silicon detected in the films may have come from backstreaming from the oil diffusion pump. The compressed powder ZnO sources are strongly contaminated and it would therefore be advantageous to be able to sputter from purer powder (non-compressed) sources, which necessitates an inversion of the sputtering structure and placement of the cathode below the substrate. This will have the added advantage of eliminating pinholes resulting from particles of large size falling on the substrate during pumpdown.

Experiments were mainly carried out in the 20-40 millitorr pressure region. This interval should be extended to include pressures as low as 5-10 millitorrs and as high as 80-120 millitorrs, since the number of collisions a particle suffers prior to deposition may play an important role. For increased cleanliness there should be as few fixtures inside the belljar as possible and stainless steel rather than aluminum or brass should be employed. A system capable of higher ultimate vacuum and an analysis of the residual gases will be decidedly helpful. Control over a wider range of substrate temperatures seems necessary and thus cooling of the substrate is indicated. The most important single observation is that reduction of the cathode size decreases the randomness in crystal orientation and further experiments should be carried out with very small or point sources.

CONCLUSIONS

An equivalent circuit model has been developed for the case of a piezoelectric transducer of finite conductivity. Calculations on the basis of this model show that :

- a.) For continuous tuning the device is essentially lossless up to conductivities as high 10^{-4} ohm-meters and for greater conductivities the mechanical to electrical conversion efficiency is higher than the electrical to mechanical conversion efficiency.
- b.) The effect of diffusion may be neglected for most practical ZnO transducers up to at least 2 GHz.
- c.) For selectively matched terminations the insertion loss is higher and is mainly the result of reflections at the input and output terminals.

A system has been designed, built, and tested for the deposition of ZnO thin films. The system constant for sputtering was inversely proportional to the oxygen content of the background gas and had its largest value for an ion incidence between 30 degrees and 40 degrees, while it exhibited an exponential dependence on substrate temperature.

The films obtained from both zinc and zinc oxide cathodes were of high resistivity and with two exceptions the c-axis of all specimens was parallel ($\pm 30^\circ$) to the substrate surface regardless of the nature of the substrate. This type of orientation has also been observed by Foster⁴ and the mechanism causing it is not yet understood. Large cathode area gave rise to an increased randomness of crystal orientation, but the films

prepared from metallic and oxide cathodes were very similar in nature. One piezoelectrically active film was obtained by the reactive sputtering of a metal source but it could not be reproduced.

To summarize, it is felt that with tighter control of conditions and some further experimentation the reactive sputtering process is capable of giving good quality, active, zinc oxide transducers.

REFERENCES

1. Nye, J.F., "Physical Properties of Crystals", Clarendon Press, Oxford, 1957.
2. Von Hippel, A., "Piezoelectricity, Ferroelectricity, and Crystal Structure",
Z. für Phys. 133, 158 (1952).
3. Berlincourt, D.A., Curran, D.R., Jaffe, H., "Piezoelectric and Piezomagnetic
Materials and Their Function in Transducers", in "Physical Acoustics"
Vol. 1, Part B, p. 169, Ed. by W.P. Mason, Academic Press, New York,
1965.
4. Watanabe, H., and Wada, M., "Optical and Electrical Properties of ZnO
Crystals", Jap. J. of Appl. Phys. 3, 617, (1964).
5. Heiland, G., Kunstmann, P., Pfister, H., "Polare Eigenschaften von Zinkoxyd-
Kristallen", Z. für Phys. 176, 485 (1963).
6. Fritsche, H., "Der Einfluss von Gelöstem Sauerstoff auf die Elektrische Leitfähig-
keit von Zinkoxyd", Z. für Phys. 133, 422 (1952).
7. Hutson, A.R., McFee, J.H., White, D.L., "Ultrasonic Amplification in CdS"
Phys. Rev. Letters 7, 237 (1961).
8. Bateman, T., "Elastic Moduli of Single-Crystal Zinc Oxide", J. Appl. Phys.
33, 3309 (1962).
9. McSkimmin, J., "Measurement of Ultrasonic Wave Velocities for Solids in the
Frequency Range of 100 to 500 Mc.", J. of Acoust. Soc. 34, 404 (1962)
IRE Transactions UE-5, 25 (1957).

10. Solbrig, C., "Piezoelektrische Messungen an Zinkoxydkristallen", *Z. für Phys.* 184, 293 (1965).
11. Hemphill, R.B., "Ultrasonic Attenuation in Zinc Oxide at Room Temperature", *Appl. Phys. Letters* 9, 35 (July 1966).
12. Hutson, A.R., "Piezoelectricity and Conductivity in ZnO and CdS", *Phys. Rev. Letters* 4, 505 (1960).
13. Heiland, G., Mollwo, E., "Electronic Processes in Zinc Oxide", *Solid State Physics*, Vol. 8, p. 191, Ed. by F. Seitz, Academic Press, New York (1959).
14. Hutson, A.R., "Hall Effect Studies of Doped Zinc Oxide Single Crystals", *Phys. Rev.* 108, 222 (1957).
15. Michelsen, R.A., "Preparation and Properties of Noncrystalline Zinc Oxide Films", *J. Appl. Phys.*, 37, 3541 (1966).
16. Dietz, R.E., Hopfield, J.J., Thomas, D.G., "Excitons and the Absorption Edge of ZnO", *J. Appl. Phys.*, 32, 2282 (1961).
17. Callen, H.B., "Thermodynamics", Wiley and Sons, (1960).
18. Kay, E., "Impact Evaporation and Thin Film Growth in A Glow Discharge", *Advances in Electronics and Electron Physics*, Vol. 17, p. 245. Ed. by L. Morton, Academic Press, N.Y., (1962).
19. Von Hippel, A., "Kathodenzerstäubungsprobleme", "Zur Theorie der Kathodenzerstäubung", *Ann. der Phys.*, 81, 1043 (1926).

20. Townes, C.H., "Theory of Cathode Sputtering in Low Voltage Gaseous Discharges",
Phys. Rev. Series II, 65, 319 (1944).
21. Seelinger, R., Sommermeyer, K., "Bemerkung zur Theorie der Kathodenzerstäubung",
Z. für Phys. 93, 692 (1935).
22. Wehner, G.K., "Controlled Sputtering of Metals by Low Energy Hg Ions", Phys.
Rev. 102, 690 (1956).
23. Moore, W.J., "The Ionic Bombardment of Solid Surfaces", Am. Scientist 48,
109 (1960).
24. Wehner, G.K., "Sputtering of Metal Single Crystals by Ion Bombardment", J.
Appl. Phys. 26, 1056 (1955).
25. Garber, R.I., Fedorenko, A.I., "Focussing of Atomic Collisions in Crystals"
Sov. Phys. Ushpeki, 479, Jan. 1965.
26. Keywell, F., "Measurements and Collision - Radiation Damage Theory of High
Vacuum Sputtering", Phys. Rev. 97, 1611 (1955).
27. Holland, L., "Vacuum Deposition of Thin Films", Wiley, (1961).
28. Grant, W.A., Carter, G., "Ion Trapping and Gas Release Phenomena", Vacuum,
15, 477 (1965).
29. Anderson, G.S., Mayer, W.N., Wehner, G.K., "Sputtering of Dielectrics by
High Frequency Fields", J. Appl. Phys. 33, 2991 (1962).
30. Hutson, A.R., White, D.A., "Propagation of Elastic Waves in Piezoelectric
Semiconductors", J. Appl. Phys. 33, 40 (1962).

31. Mollwo, E., "Quantitatives zur Lichtelektrischen Leitung in Zinkoxyd", Ann. der Phys., Band 3, 6, 230 (1948).
32. Crisler, D.F., Cupal, J.J., Moore, A.R., "Dielectric Piezoelectric and Electro-Mechanical Coupling Constants of ZnO Crystals", Proc. IEEE, 56, 225 (1968).
33. Tolansky, S., "Surface Microtopography", Wiley (Interscience) N.Y. (1960).
34. Eggers, F., "Ultrasonic Delay Line Insertion Loss Measurements in The UHF Range", IRE Trans. UE-9, p. 38, Dec. 1962.
35. Mainel, L., "Deposition of Thin Films by Cathode Sputtering", in Physics of Thin Films, Vol. 3, Ed. by G. Haas, Academic Press, (1966).
36. Foster, N.F., Rozgony, G.A., "Zinc Oxide Film Transducers", Appl. Phys. Letters, 8, 221 (1966).
37. Jaffe, H., Berlincourt, D.A., "Piezoelectric Transducer Materials", Proc. IEEE, 53, 1384 (1965).
38. May Jr., J.E., "Electronic Signal Amplification In the UHF Range with the Ultrasonic Traveling Wave Amplifier", Proc. IEEE, 53, 1465 (1965).
39. Foster, N.F., "Cadmium Sulphide Evaporated Layer Transducers", Proc. IEEE, 56, 1400 (1965).
40. de Klerk, J., Kelly, E.F., "Vapour Deposited Thin Film Piezoelectric Transducers", Rev. Sci. Instr., 36, 506 (1965).
41. Wanuga, S., Milford, T.A., Dietz, J.P., "Zinc Oxide Film Transducers", IEEE Ultrasonic Symposium, Boston, (1965).